

Ground-state phases of the spin-1 J_1 - J_2 Heisenberg antiferromagnet on the honeycomb lattice

P. H. Y. Li* and R. F. Bishop†

*School of Physics and Astronomy, Schuster Building,
The University of Manchester, Manchester, M13 9PL, UK*

We study the zero-temperature quantum phase diagram of a spin-1 Heisenberg antiferromagnet on the honeycomb lattice with both nearest-neighbor exchange coupling $J_1 > 0$ and frustrating next-nearest-neighbor coupling $J_2 \equiv \kappa J_1 > 0$, using the coupled cluster method implemented to high orders of approximation, and based on model states with different forms of classical magnetic order. For each we calculate directly in the bulk thermodynamic limit both ground-state low-energy parameters (including the energy per spin, magnetic order parameter, spin stiffness coefficient, and zero-field uniform transverse magnetic susceptibility) and their generalized susceptibilities to various forms of valence-bond crystalline (VBC) order, as well as the energy gap to the lowest-lying spin-triplet excitation. In the range $0 < \kappa < 1$ we find evidence for four distinct phases. Two of these are quasiclassical phases with antiferromagnetic long-range order, one with 2-sublattice Néel order for $\kappa < \kappa_{c1} = 0.250(5)$, and another with 4-sublattice Néel-II order for $\kappa > \kappa_{c2} = 0.340(5)$. Two different paramagnetic phases are found to exist in the intermediate region. Over the range $\kappa_{c1} < \kappa < \kappa_c^i = 0.305(5)$ we find a gapless phase with no discernible magnetic order, which is a strong candidate for being a quantum spin liquid, while over the range $\kappa_c^i < \kappa < \kappa_{c2}$ we find a gapped phase, which is most likely a lattice nematic with staggered dimer VBC order that breaks the lattice rotational symmetry.

PACS numbers: 75.10.Jm, 75.10.Kt, 75.30.Kz, 75.40.Cx

I. INTRODUCTION

The interactions between the spins of classical spin-lattice models, in which the sites of a specified infinite, regular, periodic lattice are all occupied by classical spins, typically lead to magnetic ground-state (GS) phases with perfect long-range order (LRO). While the actual GS phase that is realized depends on the precise values of the exchange coupling constants (and/or any other parameters) in the model Hamiltonian, such phases generically comprise coplanar spiral configurations with a given ordering wave vector \mathbf{Q} , for the simplest case of Bravais lattices, for example, except for some special values of \mathbf{Q} for which the GS phase may be degenerate. When the classical spins in such a model are replaced by quantum spins with a specific value of the spin quantum number s , quantum fluctuations can either reduce the corresponding magnetic order parameter M so that each sublattice of the quasiclassical GS phase retains a (nonzero) extensive magnetization or, in the more extreme case, destroy the classical LRO altogether in favor of some alternate GS phase.

Since the classical problem corresponds to the limit $s \rightarrow \infty$ of the respective quantum problem, the effect of quantum fluctuations can firstly be examined in spin-wave theory (SWT) by making power-series expansions in the parameter $1/s$. In the lowest-order SWT (LSWT) one typically finds that M is reduced from its classical value, but remains nonzero. If the model Hamiltonian is

also invariant under the continuous $SU(2)$ spin-rotation symmetry group, as is the case for all two-body Hamiltonians in which all interactions between each pair of spins considered are of Heisenberg exchange type (i.e., of the type we study henceforth), it often occurs that the classical GS phase in some region of the Hamiltonian parameter space has infinite degeneracy. In such cases the effect of quantum fluctuations at the level of LSWT is often also to lift the accidental GS degeneracy, either wholly or partially, by the order by disorder mechanism [1–3], in favor of just one or several of the classical infinitely degenerate family (IDF) of states.

In order to maximize the possibility for destroying magnetic LRO we need to introduce and optimize (geometric or dynamic) frustration between the exchange interactions present in the model, so that not all energy terms can be simultaneously minimized, and/or to enhance the quantum fluctuations. A combination of both is clearly ideal. In order to enhance the role of quantum fluctuations we clearly need to be as far removed from the classical limit as possible. In broad terms quantum fluctuations are larger for lower values of both the spin quantum number s and the lattice spatial dimensionality d . For a given value of d , quantum fluctuations are typically also larger for lattices with smaller values of the coordination number z .

Clearly, the quasiclassical magnetically-ordered GS phases discussed above spontaneously break both $SU(2)$ spin-rotation and time-reversal symmetries. Goldstone's theorem then implies that any such state breaking spin-rotational symmetry must have a vanishing energy gap. For the quasiclassical states with magnetic LRO the corresponding gapless Goldstone modes are just the spin-

* peggyhyli@gmail.com

† raymond.bishop@manchester.ac.uk

wave excitations or magnons.

On the other hand, such intrinsically quantum-mechanical states as the various forms of valence-bond crystalline (VBC) solid phases, in each of which specific, regular periodic multiplets of the lattice spins form spin singlets, are gapped and have zero magnetic order. They break neither $SU(2)$ spin-rotation symmetry nor time-reversal symmetry, while still breaking some lattice symmetries. Other states, such as multipolar or spin-nematic phases, also exist for which the $SU(2)$ spin-rotation symmetry is still broken, but in which time-reversal symmetry is preserved, thereby again excluding magnetic LRO. Finally, there exists also the possibility, in principle of quantum spin-liquid (QSL) phases that preserve *all* of the symmetries, including the lattice symmetries.

Such featureless paramagnetic states [4] as gapped QSL states, which are both fully symmetric and unfractioalized, are particularly interesting, since their existence for some specific broad classes of models is often strictly forbidden. An example of such a constraint is the Lieb-Schultz-Mattis theorem [5] for $d = 1$ chains and its extensions to systems with $d > 1$ [6, 7]. These preclude the possibility of a spin-lattice model with half-odd-integral spin per unit cell being a short-ranged gapped paramagnet that is fully symmetric and unfractioalized. Such models must be gapless, break a symmetry, or have fractionalized excitations with corresponding topological order. It is presently unknown what might be the most general such restriction to preclude short-ranged, gapped, and unfractioalized GS phases with symmetries including global $SU(2)$ spin-rotational symmetry, time-reversal symmetry, lattice translational and rotational symmetries, and other possible lattice point-group symmetries. There are also, however, various field-theoretical arguments that tend to disfavor their existence (see, e.g., Refs. [4, 8, 9]). For both these reasons it is of great interest to examine models where they are not specifically excluded by any existing theorems and, possibly, also for which idealized, candidate wave functions can be constructed [4].

The question then arises as to what are the optimal choices of possible candidate systems that might exhibit such gapped, featureless, paramagnetic GS phases. The Mermin-Wagner theorem [10] itself disallows GS magnetic LRO in isotropic Heisenberg systems for both the cases of $d = 1$ chains, even at zero temperature ($T = 0$), and $d = 2$ lattices at all nonzero temperatures ($T > 0$). Thus two-dimensional (2D) spin-lattice models at $T = 0$ provide a rich hunting-ground for exotic GS phases with no classical counterparts, and their GS quantum phase structures occupy a special place for the study of quantum phase transitions (QPTs), as a large amount of work in recent years attests. Within this class the honeycomb lattice occupies a key position for two reasons: (a) it has the lowest coordination number ($z = 3$) of all regular 2D periodic lattices, and hence is expected, *a priori*, to exhibit the largest quantum fluctuations when populated with lattice spins; and (b) it is a non-Bravais lattice (with

two sites per unit cell), to which the Lieb-Mattis theorem [5] and its relevant known extensions [6, 7] do not therefore apply.

In order to introduce frustration on the honeycomb lattice it suffices to examine the J_1 - J_2 model with antiferromagnetic (AFM) isotropic Heisenberg exchange interactions between pairs of nearest-neighbor (NN) and next-nearest-neighbor (NNN) spins with exchange coupling strengths $J_1 > 0$ and $J_2 > 0$, respectively. The J_1 - J_2 - J_3 model, which also includes isotropic Heisenberg exchange interactions between pairs of next-next-nearest-neighbor (NNNN) spins with coupling strength $J_3 > 0$, is another possibility, especially along the line $J_3 = J_2$, which includes the point of maximum classical frustration, at $J_3 = J_2 = \frac{1}{2}J_1$, where the three classical phases that the model exhibits in the sector $J_i > 0$ ($i = 1, 2, 3$) meet at a triple point, and where the classical GS phase has macroscopic degeneracy.

The spin- $\frac{1}{2}$ J_1 - J_2 - J_3 honeycomb-lattice model, or particular cases of it (e.g., when $J_3 = J_2$ or $J_3 = 0$), have been much studied using a variety of theoretical tools [11–34]. Of particular relevance for the present paper, we note that the coupled cluster method (CCM) has been extensively employed [19, 25–29] to study the $T = 0$ quantum phase structure of the model. By contrast, there are far fewer studies of the model in the case $s > \frac{1}{2}$. A specific exception is a recent study [35] of the J_1 - J_2 honeycomb-lattice model for the case $s = 1$, which used the density-matrix renormalization group (DMRG) method. Our specific aim here is to extend earlier work, which applied the CCM to the spin- $\frac{1}{2}$ version of the J_1 - J_2 honeycomb-lattice model [26, 29], to its spin-1 counterpart. While there is a broad consensus about many of the features of the $T = 0$ phase diagram of the spin- $\frac{1}{2}$ model, there is still real uncertainty about the existence of a possible QSL phase, as we discuss in more detail in Sec. II below. A main goal of the present work is to examine the possibility of any similar QSL phase in the spin-1 model.

Before discussing the model itself, however, it is interesting to note that there exists a variety of quasi-2D materials that can be regarded as experimental realizations of frustrated honeycomb-lattice systems with AFM exchange interactions. For example, the $s = \frac{1}{2}$ Cu^{2+} ions in each of such magnetic compounds as $\text{Na}_3\text{Cu}_2\text{SbO}_6$ [36], $\text{InCu}_{2/3}\text{V}_{1/3}\text{O}_3$ [37], $\beta\text{-Cu}_2\text{V}_2\text{O}_7$ [38] and Cu_5SbO_6 [39] are situated on the sites of weakly coupled honeycomb-lattice layers. Also, the iridates A_2IrO_3 ($\text{A} = \text{Na}, \text{Li}$) [40–43] are believed to be magnetically ordered Mott insulator materials in which the Ir^{4+} ions, which are disposed in weakly coupled honeycomb-lattice layers, have effective $s = \frac{1}{2}$ moments. The two families of compounds $\text{BaM}_2(\text{XO}_4)_2$ ($\text{M} = \text{Co}, \text{Ni}$; $\text{X} = \text{P}, \text{As}$) [44] and $\text{Cu}_3\text{M}_2\text{SbO}_6$ ($\text{M} = \text{Co}, \text{Ni}$) [45] also comprise similar quasi-2D materials, in each of which the magnetic M^{2+} ions occupy the sites of weakly coupled honeycomb-lattice layers. In both of these families the magnetic Ni^{2+} ions are believed to take the high-spin value $s = 1$. By

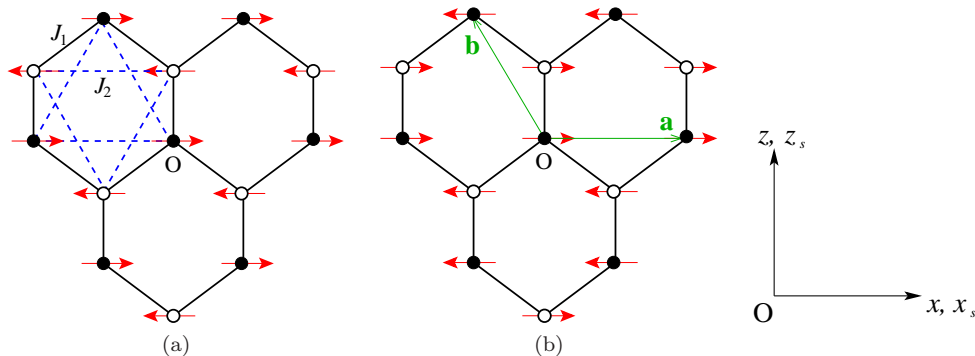


FIG. 1. (Color online) The J_1 - J_2 model on the honeycomb lattice, showing (a) the bonds ($J_1 = \text{—}$; $J_2 = \text{- - -}$), and the Néel state, and (b) one of the three Néel-II states and the triangular Bravais lattice vectors \mathbf{a} and \mathbf{b} . Sites on the two triangular sublattices \mathcal{A} and \mathcal{B} are shown by filled and empty circles respectively, and the spins are represented by the (red) arrows on the lattice sites.

contrast, the Co^{2+} ions seem to take the low-spin value $s = \frac{1}{2}$ in the former family $\text{BaCo}_2(\text{XO}_4)_2$, and the high-spin value $s = \frac{3}{2}$ in the latter compound $\text{Cu}_3\text{Co}_2\text{SbO}_6$.

In Sec. II we now describe the model itself and discuss both its classical ($s \rightarrow \infty$) limit and the results obtained to date for the extreme quantum limiting case, $s = \frac{1}{2}$. In Sec. III we give a brief description of the salient features of the CCM that we use here to discuss the $s = 1$ model. The results that we obtain are presented in Sec. IV, and we conclude with a discussion and summary in Sec. V.

II. THE MODEL

The Hamiltonian of the J_1 - J_2 model studied here is given by

$$H = J_1 \sum_{\langle i,j \rangle} \mathbf{s}_i \cdot \mathbf{s}_j + J_2 \sum_{\langle\langle i,k \rangle\rangle} \mathbf{s}_i \cdot \mathbf{s}_k, \quad (1)$$

where the operator $\mathbf{s}_i \equiv (s_i^x, s_i^y, s_i^z)$ is the quantum vector spin operator on lattice site i , with $\mathbf{s}_i^2 = s(s+1)$, and we shall be interested here in performing calculations for the case $s = 1$. The sums over $\langle i,j \rangle$ and $\langle\langle i,k \rangle\rangle$ run over all NN and NNN bonds, respectively, counting each bond once only in each sum. The parameters J_1 and J_2 are, respectively, the NN and NNN exchange couplings. We consider the case with both bonds being AFM in nature. Hence, with no loss of generality, we may, if we wish, put $J_1 \equiv 1$ to set the overall energy scale, and define $\kappa \equiv J_2/J_1$ to be the frustration parameter. The honeycomb lattice is non-Bravais with two sites per unit cell. It is composed of two interlacing triangular Bravais sublattices \mathcal{A} and \mathcal{B} . Each site on a given sublattice thus has 3 NN sites on the other sublattice and 6 NNN sites on the same sublattice. The lattice and the exchange bonds are shown in Fig. 1(a). We define the NN lattice spacing on the honeycomb lattice to be d .

The GS phase of the classical ($s \rightarrow \infty$) honeycomb lattice J_1 - J_2 model is the Néel state shown in Fig.

1(a) for values of the frustration parameter in the range $0 \leq \kappa < \frac{1}{6}$. For $\kappa > \frac{1}{6}$ the classical spins are spirally ordered, where the model has a one-parameter IDF of incommensurate GS phases in which the spiral wave vector can orient in an arbitrary direction. In LSWT spin-wave fluctuations then lift this accidental degeneracy in favor of particular wave vectors [14], leading to spiral order by disorder. In fact, for the larger J_1 - J_2 - J_3 model, with all three interactions AFM in nature and $J_3 \equiv \lambda J_1$, the line segment $\frac{1}{6} \leq \kappa \leq \frac{1}{2}$, $\lambda = 0$ marks the GS $T = 0$ phase boundary between two different spiral phases, known as the spiral-I and spiral-II phases. The (κ, λ) points $(\frac{1}{6}, 0)$ and $(\frac{1}{2}, 0)$ are tricritical points of the J_1 - J_2 - J_3 model [13]. The two spiral phases meet the Néel phase at the former tricritical point, while at the latter one they meet another classical collinear AFM phase denoted here as the Néel-II phase and illustrated in Fig. 1(b). For the J_1 - J_2 model both spiral phases are degenerate for $\frac{1}{6} < \kappa < \frac{1}{2}$, while for $\kappa > \frac{1}{2}$ only the spiral-I phase forms the stable GS phase.

Both the Néel and Néel-II states comprise sets of parallel AFM zigzag (or sawtooth) chains along one of the three equivalent honeycomb directions. While the NN spins on adjacent chains are also antiparallel for the Néel state, they are parallel for the Néel-II states. There are thus three equivalent Néel-II states, each of which has a 4-sublattice (i.e., a 4-site unit cell) structure and each of which breaks the lattice rotational symmetry. The Néel-II state is sometimes also referred to as a collinear striped AFM phase in the literature (see, e.g., Ref. [35]), for reasons which should be apparent from Fig. 1(b). However, we prefer to preserve this name (see, e.g., Ref. [28]) for yet a different classical collinear AFM state, which comprises sets of parallel ferromagnetic zigzag chains along one of the three equivalent honeycomb directions, with alternating chains having their spins aligned in opposite directions. Thus, equivalently, the striped, Néel-II, and Néel states have, in our nomenclature, 1, 2, and all 3 NN spins to a given spin antiparallel to it, respectively.

For the classical J_1 - J_2 - J_3 model on the honeycomb lattice with all 3 exchange bonds AFM in nature there is a third tricritical point in the $\kappa\lambda$ plane at $(\frac{1}{2}, \frac{1}{2})$, at which the Néel, striped, and spiral-I phases meet [13]. In fact there exist two IDFs of non-coplanar classical states, one each of which is degenerate in energy with the Néel-II and striped states, respectively, but both thermal and quantum fluctuations select the collinear configurations [13].

For the quantum models (with finite values of s) one expects, *a priori*, that quantum fluctuations will tend to destroy the spiral order over a wide window of values of the frustration parameter κ . Indeed, this has been verified by a large variety of calculations for the spin- $\frac{1}{2}$ case. For example, the CCM technique used here has shown that spiral order is destroyed over the entire range $0 \leq \kappa \leq 1$ for the spin- $\frac{1}{2}$ J_1 - J_2 model on the honeycomb lattice [26, 29].

For the spin- $\frac{1}{2}$ J_1 - J_2 honeycomb-lattice model it is by now very well established that the state with quasiclassical Néel order is the stable GS phase for $\kappa \lesssim 0.2$ (see, e.g., Refs. [21, 22, 24, 26, 29–34]). For example, the CCM technique employed here yields the value $\kappa_{c_1} = 0.207(3)$ for the corresponding quantum critical point (QCP) at which Néel order melts.

It is also reasonably well established that for values of the frustration parameter $\kappa \gtrsim 0.4$ the stable GS phase has either the Néel-II order that occurs in the classical J_1 - J_2 model only at the isolated and highly degenerate critical point $\kappa = \frac{1}{2}$, or has staggered dimer VBC (SDVBC) lattice-nematic order (see, e.g., Refs. [13, 14, 18, 20, 21, 24, 26, 29–32]). The SDVBC phase is one in which the ferromagnetic bonds (i.e., the parallel NN spin pairs) of the Néel-II states, one of which is shown in Fig. 1(b), are replaced by spin-singlet dimers. The Néel-II and SDVBC phases thus both break the same lattice rotational symmetry. The CCM technique, for example, finds a second QCP in the spin- $\frac{1}{2}$ J_1 - J_2 model on the honeycomb lattice at a value $\kappa_{c_2} = 0.385(10)$ [26, 29], beyond which the stable GS phase has SDVBC order out to a third QCP at $\kappa_{c_3} = 0.65(5)$ [29], immediately above which the stable GS phase has quasiclassical Néel-II order. This value for κ_{c_2} is in good agreement with the result $\kappa_{c_2} \approx 0.375(25)$ from a large-scale exact diagonalization (ED) study [21], and the estimates $\kappa_{c_2} \approx 0.35 - 0.36$ from three separate DMRG studies [30, 31, 33]. Whereas the ED study [21] finds a first-order transition at κ_{c_2} to a state that cannot be distinguished between having Néel-II or SDVBC order, the DMRG studies [30, 31] both favor a transition to an SDVBC phase. By contrast, another study using an entangled-plaquette variational (EPV) ansatz [24], which employs a very broad class of entangled-plaquette states, finds that the stable GS phase for $\kappa > \kappa_{c_2} \approx 0.4$ has Néel-II quasiclassical order. Lastly, two recent Schwinger boson mean-field (SB-MFT) studies [32, 34] disagree with one another on the nature of the GS phase for $\kappa \gtrsim 0.4$. Zhang and Lamas [32] find SDVBC order only in the very narrow range

$0.3732 \lesssim \kappa \lesssim 0.398$, with spiral order for $\kappa \gtrsim 0.398$. By contrast, Yu *et al.* [34] find Néel-II order for $\kappa \gtrsim 0.43$.

The region of greatest interest, and greatest uncertainty, for the $s = \frac{1}{2}$ model remains the region $\kappa_{c_1} < \kappa < \kappa_{c_2}$. For example, both SB-MFT studies [32, 34] find a transition at κ_{c_1} to a QSL state. The EPV study [24] also favors a disordered QSL phase. On the other hand, it is quite well established both from ED [13, 21] and CCM [19, 28] studies that the spin- $\frac{1}{2}$ honeycomb-lattice model exhibits a quantum paramagnetic phase with strong plaquette VBC (PVBC) order in the intermediate regime in the presence of additional AFM NNNN coupling, $J_3 > 0$. However, whether this PVBC order is maintained as $J_3 \rightarrow 0$ is more open to doubt, with various scenarios being possible. These include both PVBC and QSL states, as well as a QCP between the Néel and PVBC phases. In this context it is particularly interesting to review the results in the intermediate regime from applying the more systematic, less inherently biased, and potentially more accurate methods that have been applied to the spin- $\frac{1}{2}$ honeycomb-lattice J_1 - J_2 model, *viz.*, the DMRG method [30, 31, 33] and the CCM [26, 29].

Of the DMRG studies, Ganesh *et al.* [30] found a PVBC phase over the region $0.22 \lesssim \kappa \lesssim 0.35$, with both transitions being continuous and thus indicative of deconfined quantum criticality [46, 47]. On the other hand, Zhu *et al.* [31] found Néel order to vanish at $\kappa \approx 0.26$, and they suggested that in the region $0.26 \lesssim \kappa \lesssim 0.36$ the system either has weak PVBC order or is quantum critical. The narrow window $0.22 \lesssim \kappa \lesssim 0.26$ in which the discrepancy between these two DMRG studies occurs was the particular focus of a third DMRG study by Gong *et al.* [33]. They found Néel order to vanish at a value $\kappa \approx 0.22$, with a possible PVBC ordering in the region $0.25 \lesssim \kappa \lesssim 0.35$. They found that both magnetic (spin) and dimer orderings vanish in the thermodynamic limit in the narrow range $0.22 \lesssim \kappa \lesssim 0.25$, consistent with a possible QSL phase of the sort that other studies [15, 18, 24, 34] favor. The CCM studies [26, 29] find a paramagnetic phase in the region $\kappa_{c_1} < \kappa < \kappa_{c_2}$, with the transition at $\kappa_{c_1} = 0.207(3)$ of the continuous deconfined type, while that at $\kappa_{c_2} = 0.385(10)$ is of first-order type. While Néel order melts at κ_{c_1} , it was found [26] that PVBC order did not set in until the slightly higher value $\kappa \approx 0.24$, and the CCM study also thereby indicated a possible QSL phase in the narrow window $0.21 \lesssim \kappa \lesssim 0.24$, in broad agreement with the latest large-scale DMRG study [33].

In view of this very interesting situation for the spin- $\frac{1}{2}$ J_1 - J_2 model on the honeycomb lattice in the paramagnetic region $\kappa > \kappa_{c_1}$, beyond which Néel order melts, especially with regard to the possible existence of a (likely, very narrow) sub-regime where a QSL forms the stable GS phase, it is clearly of great interest to study its spin-1 counterpart. To that end we employ here the same CCM technique as has been used for the spin- $\frac{1}{2}$ model [26, 29] to considerable effect, as discussed above. We will calculate a complete set of low-energy parameters, including

the GS energy per spin E/N , the magnetic order parameter (i.e., the relevant sublattice magnetization) M , the spin stiffness ρ_s , and the zero-field (uniform, transverse) magnetic susceptibility χ , in order to build up as much information as possible about the $T = 0$ quantum phase diagram of the model. We also calculate the triplet spin gap Δ . Before presenting our results in Sec. IV we first give a brief discussion of the key ingredients of the CCM itself, including the reference states we employ to calculate the various low-energy parameters.

III. THE COUPLED CLUSTER METHOD

We briefly review the most important elements of the CCM, and refer the interested reader to the extensive literature (and see, e.g., Refs. [48–58] and references cited therein) for further details. As we shall see, the method is size-extensive at all levels of implementation, and hence directly provides results in the (thermodynamic) infinite-lattice limit, $N \rightarrow \infty$. The first step is always the choice of a suitable (normalized) many-body reference state (or model state) $|\Phi\rangle$, with respect to which the exact many-body GS wave function $|\Psi\rangle$ may be parametrized via a systematic scheme to incorporate the correlations, which we describe below. We use here, for example, the quasi-classical Néel and Néel-II collinear AFM states shown in Figs. 1(a) and 1(b), respectively, as suitable model states, among others described below too. Broadly speaking, the role of any CCM model state $|\Phi\rangle$ is that of a generalized vacuum state. The precise properties needed of a model state are described in detail below.

The exact ket GS wave function $|\Psi\rangle$ and its bra counterpart $\langle\tilde{\Psi}|$ satisfy the normalization conditions,

$$\langle\tilde{\Psi}|\Psi\rangle = \langle\Phi|\Psi\rangle = \langle\Phi|\Phi\rangle \equiv 1. \quad (2)$$

They satisfy their respective GS Schrödinger equations,

$$H|\Psi\rangle = E|\Psi\rangle; \quad \langle\tilde{\Psi}|H = E\langle\tilde{\Psi}|. \quad (3)$$

In terms of a suitably chosen model state $|\Phi\rangle$ they are parametrized within the CCM by the characteristic exponentiated forms,

$$|\Psi\rangle = e^S|\Phi\rangle; \quad \langle\tilde{\Psi}| = \langle\Phi|\tilde{S}e^{-S}. \quad (4)$$

Hermiticity clearly implies the explicit relation,

$$\langle\Phi|\tilde{S} = \frac{\langle\Phi|e^{S^\dagger}e^S}{\langle\Phi|e^{S^\dagger}e^S|\Phi\rangle}, \quad (5)$$

between the two CCM GS correlation operators \tilde{S} and S .

Nevertheless, another key feature of the CCM is that the constraint implied by Eq. (5) is *not* explicitly imposed. Instead, the two correlation operators are formally decomposed independently as the two sums,

$$S = \sum_{I \neq 0} S_I C_I^+; \quad \tilde{S} = 1 + \sum_{I \neq 0} \tilde{S}_I C_I^-, \quad (6)$$

in which $C_0^+ \equiv 1$ is the identity operator in the corresponding many-body Hilbert (or Fock) space, and where I is a set index that captures a complete set of single-body configurations for all N particles. More specifically, what is mathematically required of $|\Phi\rangle$ is that it is a cyclic (or fiducial) vector with respect to a complete set of multiconfigurational (many-body) creation operators $\{C_I^+\}$, all of which, very importantly, are chosen so as to mutually commute between themselves,

$$[C_I^+, C_J^+] = 0, \quad \forall I, J \neq 0. \quad (7)$$

Hence, the set of states $\{C_I^+|\Phi\rangle\}$ forms a complete basis for the ket-state Hilbert space. Furthermore, the state $|\Phi\rangle$ also has the property that it is a generalized vacuum state with respect to the set of operators $\{C_I^-\}$, so that

$$\langle\Phi|C_I^+ = 0 = C_I^-|\Phi\rangle, \quad \forall I \neq 0, \quad (8)$$

where the corresponding multiconfigurational destruction operators, $C_I^- \equiv (C_I^+)^\dagger$, similarly span the bra-state Hilbert space in the sense that the set of states $\{\langle\Phi|C_I^-\}$ forms a complete basis for it.

These rather general parametrizations encapsulated in Eqs. (4), (6)–(8) form the core of the CCM, and have several immediate consequences. At first sight it might appear to be a drawback of the method that Hermiticity is not imposed via Eq. (5). While the exact CCM correlation operators of Eq. (6) will surely fulfill Eq. (5) exactly, when approximations are made in practice (e.g., by truncating the sums over configurations I in Eq. (6) to some suitable, manageable subset) the Hermiticity relation may only be satisfied approximately. In turn this will have the consequence that the GS energy estimates obtained at any approximate level of implementation of the CCM, as described more fully below, do not automatically provide strict upper bounds to the true GS energy. We return to this point in Sec. V after presenting our results. Nevertheless, this potential disadvantage is almost always far outweighed in practice by several advantages that similarly flow from the CCM parametrization scheme.

One very important such advantage is that the scheme itself implies that the Goldstone linked-cluster theorem will always be exactly preserved, even when the sums in Eq. (6) are arbitrarily truncated, as we demonstrate explicitly below. As an immediate consequence, the CCM is thus size-extensive at any such approximate level of implementation. Hence, all thermodynamically extensive variables, such as the GS energy E , scale linearly with N at arbitrary levels of approximation, thereby allowing us to work from the outset in the thermodynamic limit ($N \rightarrow \infty$), and obviating the need for any finite-size scaling of the numerical results that is required in most alternative techniques. A second key advantage of the CCM, which similarly stems as an immediate consequence of the exponentiated parametrization scheme, is that it also exactly preserves the very important Hellmann-Feynman theorem at all similar levels of implementation as above.

Clearly, all GS information of the system is obtainable from the CCM c -number correlation coefficients $\{\mathcal{S}_I, \tilde{\mathcal{S}}_I\}$, which may themselves now formally be calculated by minimizing the GS energy functional,

$$\bar{H} = \bar{H}[\mathcal{S}_I, \tilde{\mathcal{S}}_I] \equiv \langle \Phi | \tilde{S} e^{-S} H e^S | \Phi \rangle, \quad (9)$$

from Eq. (4), with respect to each of the parameters $\{\mathcal{S}_I, \tilde{\mathcal{S}}_I; \forall I \neq 0\}$. Variation of \bar{H} with respect to the coefficient $\tilde{\mathcal{S}}_I$ thus yields the set of conditions,

$$\langle \Phi | C_I^- e^{-S} H e^S | \Phi \rangle = 0, \quad \forall I \neq 0, \quad (10)$$

while variation with respect to the coefficient \mathcal{S}_I yields the corresponding set of conditions,

$$\langle \Phi | \tilde{S} e^{-S} [H, C_I^+] e^S | \Phi \rangle = 0, \quad \forall I \neq 0. \quad (11)$$

Equation (10) is a coupled set of nonlinear equations for the set of GS ket coefficients $\{\mathcal{S}_I, \forall I \neq 0\}$, while Eq. (11) is a coupled set of linear equations for the set of GS bra coefficients $\{\tilde{\mathcal{S}}_I, \forall I \neq 0\}$ once the ket coefficients $\{\mathcal{S}_I, \forall I \neq 0\}$ are used as input, having been found first from solving Eq. (10). Both Eqs. (10) and (11) have the same number of equations as unknown parameters to be solved for.

The GS energy E is now simply the value of \bar{H} from Eq. (9) at the extremum obtained from Eqs. (10) and (11),

$$E = \langle \Phi | e^{-S} H e^S | \Phi \rangle = \langle \Phi | H e^S | \Phi \rangle. \quad (12)$$

While E , uniquely, is thus given in terms of the ket-state correlation coefficients $\{\mathcal{S}_I\}$ alone, the GS expectation value of any other physical operator (e.g., the sublattice magnetization M) will require a knowledge of both sets $\{\mathcal{S}_I\}$ and $\{\tilde{\mathcal{S}}_I\}$. The use of Eq. (12) in Eq. (11) also yields the equivalent set of generalized linear eigenvalue equations,

$$\langle \Phi | \tilde{S} (e^{-S} H e^S - E) C_I^+ | \Phi \rangle = 0, \quad \forall I \neq 0, \quad (13)$$

for the GS bra coefficients $\{\tilde{\mathcal{S}}_I, \forall I \neq 0\}$.

Within the CCM framework, excited-state (ES) wave functions are parametrized as

$$|\Psi_e\rangle = X^e e^S |\Phi\rangle, \quad (14)$$

where the linear excitation operator X^e is expanded as

$$X^e = \sum_{I \neq 0} \mathcal{X}_I^e C_I^+, \quad (15)$$

by analogy to Eq. (6). A simple combination of the GS ket-state Schrödinger equation (3) with its ES counterpart,

$$H |\Psi_e\rangle = E_e |\Psi_e\rangle, \quad (16)$$

readily yields the equation,

$$e^{-S} [H, X^e] e^S |\Phi\rangle = \Delta_e X^e |\Phi\rangle, \quad (17)$$

by making use of the simple commutativity relation, $[X^e, S] = 0$, which follows trivially from their definitions in Eqs. (6) and (15), and from Eq. (7), and where Δ_e is the excitation energy,

$$\Delta_e \equiv E_e - E. \quad (18)$$

By taking the overlap of Eq. (17) with $\langle \Phi | C_I^-$, we find the set of equations,

$$\langle \Phi | C_I^- [e^{-S} H e^S, X^e] | \Phi \rangle = \Delta_e \mathcal{X}_I^e, \quad \forall I \neq 0, \quad (19)$$

where we have made use of the fact that the set of states $\{C_J^+ |\Phi\rangle\}$ is (or may be constructed to be) orthonormalized,

$$\langle \Phi | C_I^- C_J^+ | \Phi \rangle = \delta(I, J), \quad \forall I, J. \quad (20)$$

These generalized eigenvalue equations (19) are then solved for the set of ket-state ES correlation coefficients $\{\mathcal{X}_I^e\}$ and the excitation energy Δ_e .

Up to this point the CCM procedure is exact. Nevertheless, one may wonder whether it is necessary in practice to truncate the infinite-series expansions for the ubiquitous exponential terms $e^{\pm S}$. However, we note that these exponentiated forms of the operator S occur in all of the equations to solve or compute [e.g., Eqs. (10)–(13), (19)] only in the combination of a similarity transformation of the Hamiltonian of the system, $e^{-S} H e^S$. This may be expanded as the well-known nested commutator series,

$$e^{-S} H e^S = \sum_{n=0}^{\infty} \frac{1}{n!} [H, S]_n, \quad (21)$$

where $[H, S]_n$, defined iteratively as

$$[H, S]_n = [[H, S]_{n-1}, S]; \quad [H, S]_0 = H, \quad (22)$$

is an n -fold nested commutator. Yet another key feature of the CCM parametrization of Eq. (6) is that this otherwise infinite sum in Eq. (21) will now (usually, as here) terminate at some low finite order, due to the mutual commutativity relation of Eq. (7) and the fact that H is (usually, as here) of finite order in the corresponding set of relevant single-particle operators, as we now explain.

In general, if H involves up to m -body interaction terms, its second-quantized form will contain products of up to $2m$ single-body creation and destruction operators, and the sum in Eq. (21) then terminates at the term with $n = 2m$. Similarly, in our present case where the Hamiltonian of Eq. (1) is bilinear in the SU(2) operators it is easy to see from the SU(2) commutation relations that Eq. (21) terminates exactly at the term with $n = 2$ when C_I^+ comprises a product of single spin-raising operators, $s_k^+ \equiv s_k^x + i s_k^y$, on various sites k , as we discuss below. We also observe that the mutual commutativity requirement of Eq. (7) on all the operators $\{C_I^+, \forall I \neq 0\}$ that comprise the decomposition of the correlation operators S in Eq. (6), has the immediate consequence that

all nonzero terms in the expansion in Eq. (21) must be linked to the Hamiltonian. It is simply not possible to generate unlinked terms in this way, and hence the Goldstone linked-cluster theorem (and its corollary of size-extensivity) is preserved even if truncations are made for the expansions in Eq. (6) of the CCM correlation operators.

Thus, finally, to implement the CCM in practice, the sole approximation made is to restrict the set of multiconfigurational set-indices $\{I\}$ that are retained in the expansions of the correlation operators $\{S, \tilde{S}, X^e\}$ in Eqs. (6) and (15) to some manageable (infinite or finite) subset. Clearly, the related choices for both the appropriate model state $|\Phi\rangle$ and the appropriate truncation scheme should be based on physical grounds, and we turn now to how such choices are made for spin-lattice models in general.

The simplest broad class of model states for quantum magnets comprises independent-spin product states, in each of which the spin projection of every spin, along some specified quantization axis on each lattice site, is independently specified. The two collinear Néel and Néel-II AFM states shown, respectively, in Figs. 1(a) and 1(b) are clearly of this type. More generally, so are all such similar quasiclassical states with perfect magnetic LRO. It is extremely convenient to put all such states on the same footing, and thereby treat them universally. One simple way to do so is to make a passive rotation of each spin independently (i.e., by choosing local spin quantization axes on each lattice site independently), so that every spin on every site then points, say, downwards, (i.e., along the negative z_s direction of the axes shown in Fig. 1) in its own local spin-coordinate frame. The basic SU(2) spin commutation relations are, of course, preserved under such unitary transformations. In this way all lattice sites become equivalent to one another, whatever the form of the independent-spin product, quasiclassical, model state $|\Phi\rangle$ that is chosen as the CCM reference state. All such states take the universal form $|\Phi\rangle = |\downarrow\downarrow\downarrow \cdots \downarrow\rangle$ in their own local spin-coordinate frames. Once such frames have been chosen, all that is needed is to re-express the Hamiltonian H in terms of them.

It is now simple also to see how to make all such states $|\Phi\rangle$ fiducial vectors with respect to a suitable set of mutually commuting many-body creation operators $\{C_I^+\}$. Thus, we may simply construct C_I^+ as a product of single-spin raising operators, $C_I^+ \rightarrow s_{k_1}^+ s_{k_2}^+ \cdots s_{k_n}^+$; $n = 1, 2, \dots, 2sN$, with the set-index I now becoming a collection of lattice-site indices, $I \rightarrow \{k_1, k_2, \dots, k_n; n = 1, 2, \dots, 2sN\}$, wherein each individual site index may appear no more than $2s$ times.

Within the CCM framework so described for quantum spin-lattice models, a very general and systematic hierarchy of approximations, called the SUB n - m scheme, has been extensively applied to a wide variety of systems, ranging from unfrustrated to highly frustrated models, with considerable success. For specified values of the

pair of positive-integral truncation indices n and m , the CCM SUB n - m approximation retains only those multispin configurations I above, which involve no more than n spin flips that span a range of up to a maximum of m contiguous sites. In this context a single spin flip requires the action of a spin-raising operator s_k^+ acting once, and a set of lattice sites is defined to be contiguous if each site in the set is NN (in the specified geometry) to at least one other in the set. Clearly, the SUB n - m approximation becomes exact as both truncation indices n and m become indefinitely large. Different sub-schemes can also be specified according to how each truncation index approaches the exact infinite limit.

A very extensively used approximation scheme is the localized (lattice-animal-based subsystem) LSUB m scheme [57, 58]. At the m th level of approximation, this scheme is defined to retain all clusters of spins described by multispin-flip configurations $\{I\}$ in the sums in Eqs. (6) and (15) that span m or fewer contiguous lattice sites. The configurations retained are thus defined on all possible lattice animals (or polyominoes, equivalently, in the usual graph-theoretic sense) of maximal size m . Clearly, the LSUB m scheme is equivalent to the previously defined SUB n - m scheme in the case $n = 2sm$, i.e., LSUB $m \equiv \text{SUB}2sm$ - m . It is precisely the LSUB m scheme that we used, for example, in our earlier studies [26, 29] of the spin- $\frac{1}{2}$, honeycomb-lattice J_1 - J_2 model.

The number $N_f = N_f(m)$ of fundamental multispin-flip configurations that are defined to be distinct under the symmetries of the lattice and the particular model state $|\Phi\rangle$ being employed (i.e., the effective size of the index set $\{I\}$), and which are retained at a given m th level of LSUB m approximation, is clearly lowest for $s = \frac{1}{2}$. Since $N_f(m)$ rises sharply for a given truncation index m as s is increased, and also since $N_f(m)$ typically increases faster than exponentially for a given value of s as m is increased, the alternative SUB n - n scheme is usually preferred for models with $s > \frac{1}{2}$, as here. Clearly, SUB n - $n \equiv \text{LSUB}n$ only for $s = \frac{1}{2}$, whereas for $s > \frac{1}{2}$ we have SUB n - $n \subset \text{LSUB}n$. For most of the calculations performed here, including all of those based on the Néel and Néel-II states as CCM model states, we employ the SUB n - n scheme up to the very high order $n = 10$.

We note that the multispin-flip cluster configurations $\{I\}$ in the expansion of Eq. (15) for the excitation operator X^e are different to those in the corresponding expansion of Eq. (6) for the GS correlations operators S and \tilde{S} . They are also different for each model state. Thus, for the ES calculations for the triplet spin gap Δ we restrict ourselves to configurations I that change the z component of total spin, S^z , by one unit, whereas for the GS calculations we restrict ourselves to those with $S^z = 0$. To ensure comparable accuracy for both the GS and ES calculations, however, we use the SUB n - n approximation in both cases. Once again, even though the number of fundamental configurations, $N_f(n)$, at a given n th level of SUB n - n approximation, is different for the ES case than for the GS case using the same CCM model state $|\Phi\rangle$, our

calculations here for Δ are also done up to the very high order $n = 10$, for both the Néel and Néel-II choices of model state. For example, for the Néel model state in the present spin-1 model, we have $N_f(10) = 219521$ for the GS case and $N_f(10) = 244533$ for the triplet spin-gap ES case. Corresponding numbers for the Néel-II model state are $N_f(10) = 630130$ and $N_f(10) = 710533$ for the GS and triplet spin-gap ES cases, respectively. Clearly, with such large numbers of equations to derive and solve [57], one needs both massive parallelization and supercomputing resources, as well as purpose-built computer-algebra packages for the derivation of the equations [59].

We are also interested here in calculating other low-energy parameters of the system, namely the spin stiffness coefficient ρ_s and the zero-field (uniform, transverse) magnetic susceptibility χ , for which suitably twisted and canted quasiclassical states, respectively, are also required as CCM model states, as we now describe. For example, the spin stiffness (or helicity modulus) ρ_s of a spin-lattice system provides a quantitative measure of the energy required to rotate the order parameter of a magnetically ordered state by an (infinitesimal) angle θ per unit length in a specified direction. Thus if the GS energy as a function of the imposed twist is $E(\theta)$, and $N(\rightarrow \infty)$ is the number of lattice sites, we have

$$\frac{E(\theta)}{N} = \frac{E}{N} + \frac{1}{2}\rho_s\theta^2 + O(\theta^4), \quad (23)$$

where $E \equiv E(\theta = 0)$. We note that θ has the dimensions of an inverse length. In the thermodynamic limit ($N \rightarrow \infty$) considered here a nonzero (positive) value of ρ_s implies the stability of the magnetic LRO of the state in question. Exceptionally, for the Néel state (illustrated in Fig. 1(a) with a staggered magnetization in the x_s direction), the value of ρ_s is completely independent of the applied twist direction, since its ordering wave vector takes the value $\mathbf{Q} = (0, 0)$ in the xz plane shown in Fig. 1. We show in Fig. 2 the twist applied in the x direction to the unperturbed Néel state of Fig. 1(a), and it is just the twisted state shown in Fig. 2 that we now use as our CCM model state to calculate ρ_s for the Néel GS phase. The definition of Eq. (23) readily yields that the corresponding classical ($s \rightarrow \infty$) value of ρ_s for the Néel state of the J_1 - J_2 model on the honeycomb lattice is

$$\rho_{s;\text{cl}}^{\text{Néel}} = \frac{3}{4}(1 - 6\kappa)J_1d^2s^2, \quad (24)$$

where d is the honeycomb lattice spacing. Unsurprisingly, $\rho_{s;\text{cl}}^{\text{Néel}} \rightarrow 0$ at precisely the point $\kappa = \frac{1}{6}$ where the classical Néel LRO vanishes, and we have a continuous transition to a stable GS phase with spiral order.

Suppose we now place our unperturbed system in an external transverse magnetic field \mathbf{h} , in order to calculate its zero-field magnetic susceptibility χ . For the two collinear, quasiclassical AFM states shown in Fig. 1, both of which have spins aligned along the x_s axis, the field is applied in the z_s direction, $\mathbf{h} = h\hat{z}_s$. In units

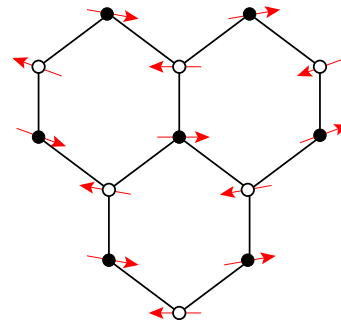


FIG. 2. (Color online) The twisted reference state for the calculation of the spin stiffness coefficient, ρ_s , for the J_1 - J_2 honeycomb model. The twist is applied in the x direction to the Néel state shown in Fig. 1(a). The spins on lattice sites \bullet are represented by the (red) arrows.

where the gyromagnetic ratio $g\mu_B/\hbar = 1$, the Hamiltonian $H = H(h = 0)$ of Eq. (1) then becomes

$$H(h) = H(0) + h \sum_l s_l^z, \quad (25)$$

In the presence of the magnetic field the spins will cant at an angle α to the x_s axis with respect to their zero-field configurations, as shown in Figs. 3(a) and 3(b) for the two quasiclassical AFM states shown in Figs. 1(a) and 1(b), respectively. For both states the classical ($s \rightarrow \infty$) value of α is readily found by minimizing the classical energy, $E = E(h)$, corresponding to Eq. (25), with respect to the cant angle α . As usual, the uniform (transverse) magnetic susceptibility is then defined as

$$\chi(h) = -\frac{1}{N} \frac{d^2 E}{dh^2}. \quad (26)$$

Its zero-field limit is then the respective low-energy parameter, $\chi \equiv \chi(0)$, and the corresponding analog of Eq. (23) is hence,

$$\frac{E(h)}{N} = \frac{E}{N} - \frac{1}{2}\chi h^2 + O(h^4). \quad (27)$$

where $E \equiv E(h = 0)$. The two canted states shown in Figs. 3(a) and 3(b) are just the CCM model states that we use to calculate χ for the Néel and Néel-II GS phases, respectively. Simple calculations show that the corresponding classical ($s \rightarrow \infty$) values for the J_1 - J_2 model on the honeycomb lattice are

$$\chi_{\text{cl}}^{\text{Néel}} = \frac{1}{6J_1}, \quad (28)$$

and

$$\chi_{\text{cl}}^{\text{Néel-II}} = \frac{1}{4(1 + 2\kappa)J_1}, \quad (29)$$

independent of s in each case classically.

Unlike the classical spin stiffness coefficient, the classical zero-field susceptibility coefficient is not expected

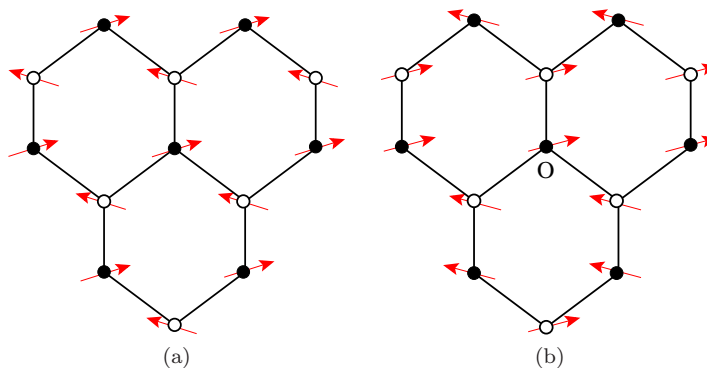


FIG. 3. (Color online) The canted reference states for the calculation of the zero-field magnetic susceptibility, χ , for the J_1 - J_2 honeycomb model. The external magnetic field is applied in the z_s direction to the (a) Néel and (b) Néel-II states shown in Figs. 1(a) and 1(b), respectively. The spins on lattice sites \bullet are represented by the (red) arrows.

to go to zero at a phase transition point where the corresponding magnetic LRO vanishes. However, the two classical values in Eqs. (28) and (29) do meet (at a finite value) at the point $\kappa = \frac{1}{4}$. This is precisely the point at which the corresponding classical energy curves,

$$\frac{E_{\text{cl}}^{\text{Néel}}}{N} = -\frac{3}{2}(1 - 2\kappa)J_1, \quad (30)$$

and

$$\frac{E_{\text{cl}}^{\text{Néel-II}}}{N} = -\frac{1}{2}(1 + 2\kappa)J_1, \quad (31)$$

cross (or, more precisely, would cross if these two GS phases were in competition with one another in the classical model). We note, however, that, unlike in the classical limit, χ *can* become zero in a quantum case (i.e., for a finite value of s) at a QCP, where it provides a clear signal of a spin gap opening [60, 61] (i.e., a transition to a gapped state).

While the CCM does not involve any finite-size scaling of its results, as a final step we do need to extrapolate our SUB n - n sequences of approximants for any GS or ES calculated physical parameter to the limit $n \rightarrow \infty$ where, by construction, the method becomes exact. Although no exact such extrapolation rules are known, by now there exists a large body of heuristic work on a very wide variety of spin-lattice models that has led to empirical schemes for many physical quantities. Thus, for example, a very well tested and highly accurate extrapolation scheme for the GS energy per spin has been shown to be (and see, e.g., Refs. [19, 25–29, 58, 62–74])

$$\frac{E(n)}{N} = e_0 + e_1 n^{-2} + e_2 n^{-4}. \quad (32)$$

As expected, the convergence as a function of the SUB n - n truncation index n of all other GS physical parameters is slower than for the energy. A typical example is the magnetic order parameter M (i.e., the appropriate

sublattice magnetization), which takes the simple form,

$$M = -\frac{1}{N} \sum_{k=1}^N \langle \Phi | \tilde{S} e^{-S} s_k^z e^S | \Phi \rangle. \quad (33)$$

in terms of the local rotated spin-coordinate frames discussed above. For unfrustrated or only very mildly frustrated systems, an extrapolation scheme for $M(n)$ with leading power $1/n$ (rather than $1/n^2$, as for the GS energy),

$$M(n) = m_0 + m_1 n^{-1} + m_2 n^{-2}, \quad (34)$$

has been found (and see, e.g., Refs. [25–27, 29, 62–65, 69–73]) to fit the CCM results extremely well. By contrast, for highly frustrated systems, a scheme which has been found to be more appropriate and to fit the CCM results very closely in a wide variety of earlier studies (and see, e.g., Refs. [19, 25–29, 66–68, 74]) is one with a leading power $1/n^{1/2}$,

$$M(n) = \mu_0 + \mu_1 n^{-1/2} + \mu_2 n^{-3/2}. \quad (35)$$

This latter scheme is particularly appropriate for systems with an order-disorder transition, or for systems which are either close to a QCP or for which M is close to zero.

CCM SUB n - n extrapolation schemes with a leading power $1/n$ have also been shown to fit the results very well for the corresponding approximants for each of the spin gap $\Delta(n)$ (and see, e.g., Refs. [63, 75–77]),

$$\Delta(n) = d_0 + d_1 n^{-1} + d_2 n^{-2}, \quad (36)$$

the spin stiffness coefficient $\rho_s(n)$ (and see, e.g., Refs. [66, 76, 78–80]),

$$\rho_s(n) = s_0 + s_1 n^{-1} + s_2 n^{-2}, \quad (37)$$

and the zero-field magnetic susceptibility, $\chi(n)$ (and see, e.g., Refs. [76, 79–81]),

$$\chi(n) = x_0 + x_1 n^{-1} + x_2 n^{-2}, \quad (38)$$

from which we obtain, respectively, the extrapolated values $\Delta \equiv \Delta(\infty) = d_0$, $\rho_s \equiv \rho_s(\infty) = s_0$, and $\chi \equiv \chi(\infty) = x_0$.

We note that each of the extrapolation schemes of Eqs. (32) and (34)–(38) contains three fitting parameters. Clearly, in order to obtain stable and robust fits to such schemes it is preferable to use at least four SUB n – n data points as input. However, occasionally this is either impracticable or inappropriate, for various reasons we describe. In such cases it is often then preferable to utilize, for the particular GS physical parameter P involved, a completely unbiased extrapolation scheme for the CCM SUB n – n approximants $P(n)$ of the form,

$$P(n) = p_0 + p_1 n^{-\nu}, \quad (39)$$

in which the leading exponent ν is itself a free fitting parameter, along with p_0 and p_1 . Naturally, it is always possible to perform such a fit first for any GS quantity, even when we have four or more data points to utilize, in order to check the value of the leading exponent, before using one of the afore-mentioned schemes of Eqs. (32) and (34)–(38).

IV. RESULTS

We will return in Sec. V, after first presenting our results, to the question of the role, in practice, of the CCM model state, and the related question of whether or not our results depend on the specific choices made. Firstly, however, we show in Fig. 4 our results for the GS energy per spin, E/N , for the model, using both the Néel and Néel-II AFM states as CCM model states. In each case we display the respective results from SUB n – n approximations with $n = \{2, 4, 6, 8, 10\}$, together with the corresponding SUB ∞ – ∞ extrapolations based on the data sets with $n = \{4, 6, 8, 10\}$ as input to Eq. (32), to find the corresponding ($n \rightarrow \infty$) extrapolated values e_0 . It is clear from Fig. 4 that for the SUB n – n calculations based on both quasiclassical AFM states, convergence is rapid as the truncation index n is increased. We also note that each of the energy curves terminates at some critical value of the frustration parameter that depends both on the model state chosen and the SUB n – n approximation used. For the curves based on the Néel model state there is an upper critical value, and for those based on the Néel-II model state a lower critical value. In both cases, for values of κ beyond the respective critical value no real solution can be found to the corresponding CCM equations (10).

Such CCM termination points of the coupled sets of SUB n – n equations are both common in practice and well understood (see, e.g., Refs. [26, 58, 69]). They are always simply a consequence of the corresponding QCP that exists in the model under study, and which marks the melting of the respective form of magnetic LRO corresponding to the particular model state used. For a given (finite) value of the SUB n – n truncation index n

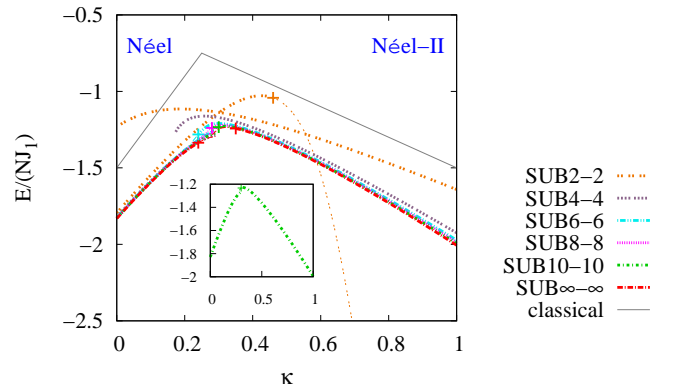


FIG. 4. (Color online) CCM results for the GS energy per spin E/N (in units of J_1) versus the frustration parameter $\kappa \equiv J_2/J_1$, for the spin-1 J_1 – J_2 model on the honeycomb lattice (with $J_1 > 0$). Results based on both the Néel and Néel-II states as CCM model states are shown in SUB n – n approximations with $n = \{2, 4, 6, 8, 10\}$, together with the corresponding SUB ∞ – ∞ extrapolations using Eq. (32), with the respective data set $n = \{4, 6, 8, 10\}$. The plus (+) symbols on the curves mark the points where the respective solutions have $M \rightarrow 0$, and those portions of the curves shown with thinner lines beyond the plus (+) symbols indicate unphysical regions where $M < 0$. For comparison we also show the corresponding classical curves from Eqs. (30) and (31) for the value $s = 1$.

and for a given phase, Fig. 4 shows that the CCM solutions extend beyond the actual (SUB ∞ – ∞) QCP into the unphysical regime beyond the QCP, as is usually the case in other models studied. The extent of the unphysical regime diminishes as the truncation index n increases, and ultimately vanishes in the exact ($n \rightarrow \infty$) limit.

Figure 4 demonstrates clear preliminary evidence for the existence of an intermediate phase between the phases with Néel and Néel-II magnetic LRO for the $s = 1$ J_1 – J_2 model, just as for its $s = \frac{1}{2}$ counterpart. For example, Fig. 4 shows that, whereas the SUB n – n GS energy results based on the Néel and Néel-II model states for a given value of n cross one another for values $n \leq 8$, before their respective termination points, this is no longer the case for $n = 10$, as the inset shows clearly, where the upper termination point for the Néel phase and the lower termination point for the Néel-II phase are both around $\kappa \approx 0.28$. Presumably, if we could perform CCM SUB n – n calculations with $n > 10$ a gap would appear between the respective termination points.

More detailed evidence for the regions of stability of the quasiclassical AFM phases with magnetic LRO, and for any intermediate phase, can clearly be obtained from the GS magnetic order parameter M of Eq. (33). Thus, in Fig. 5 we show our analogous SUB n – n results for M to those shown in Fig. 4 for E/N . Firstly, we note that, exactly as expected, the SUB n – n sequences of approxi-

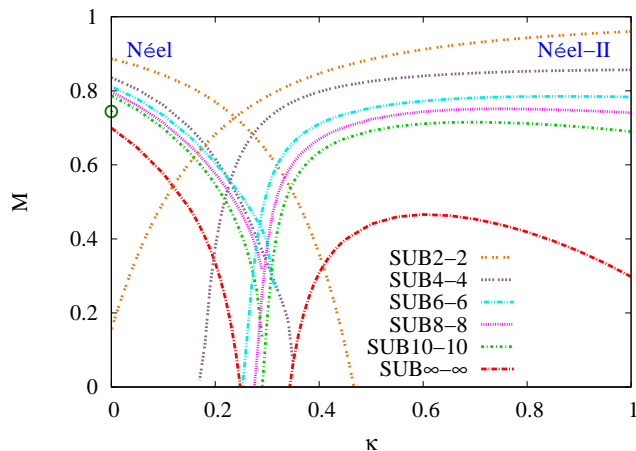


FIG. 5. (Color online) CCM results for the GS magnetic order parameter M versus the frustration parameter $\kappa \equiv J_2/J_1$, for the spin-1 J_1 - J_2 model on the honeycomb lattice (with $J_1 > 0$). Results based on both the Néel and Néel-II states as CCM model states are shown in $\text{SUB}n$ - n approximations with $n = \{2, 4, 6, 8, 10\}$, together with the corresponding $\text{SUB}\infty$ - ∞ extrapolations using Eq. (35), with the respective data set $n = \{2, 6, 10\}$. Rather than crowd the figure with additional full curves based on (the largely inappropriate) Eq. (34), we show with the circle (\circ) symbol the corresponding extrapolated value based on the Néel state using Eq. (34), with data set $n = \{2, 6, 10\}$, for the case $\kappa = 0$ only, where this extrapolation scheme *is* the appropriate one.

mations for M based on both model states converge appreciably more slowly than for E/N . Secondly, it is very interesting to note from Fig. 5 that many of the $\text{SUB}n$ - n curves for M , particularly all of those based on the Néel-II model state, become zero *before* the respective termination point. These points have been denoted by plus (+) symbols on the corresponding energy curves in Fig. 4, wherein the respective portions of the curves beyond these points where $M < 0$ are shown by thinner lines to denote that these regions are unphysical.

A third, more subtle, point can also be seen from Fig. 5. Thus, over both the entire region of the Néel-II curves and the region of the Néel curves away from the immediate vicinity of the unfrustrated $\kappa = 0$ limit, there is a marked $(4m - 2)/4m$ staggering effect for the raw $\text{SUB}n$ - n results. For example, for the Néel curves, the staggering effect is strong enough that the two $\text{SUB}n$ - n curves for M with $n = 4, 6$ even cross one another at a value $\kappa \approx 0.2$. Thus, the two $\text{SUB}n$ - n sequences of corresponding values for M at a fixed value of κ , i.e., for $n = (4m - 2)$ on the one hand and $n = 4m$ on the other, tend to converge quite differently from one another, for all positive integral values of m . Conversely, each of these sequences separately seems to converge monotonically. Such staggered (or non-monotonic) CCM $\text{SUB}n$ - n sequences have also been observed in other models. For example, for the spin- $\frac{1}{2}$ J_1 - J_2 model on the triangular lattice, it has been shown explicitly [82] that there ex-

ists corresponding $(2m - 1)/2m$ (i.e., odd/even) staggering in the CCM $\text{SUB}n$ - n sequences based on both the 3-sublattice 120° Néel state and the 2-sublattice AFM striped state as model states. In view of the fact that the present honeycomb lattice comprises two interlocking triangular Bravais sublattices, it is probable that the staggering effects observed in the J_1 - J_2 models on the honeycomb and triangular lattices are related, and consistent with one another.

It is interesting to note that a closer inspection of the CCM $\text{SUB}n$ - n results for M for the spin- $\frac{1}{2}$ version of the present honeycomb-lattice J_1 - J_2 model in Ref. [29] also reveals a similar $(4m - 2)/4m$ staggering to that observed here. In the light of the current results, one can see that that staggering effect was overlooked there, but was rather interpreted as showing that the $\text{SUB}6$ - 6 result was anomalous by comparison with the $\text{SUB}n$ - n approximants, $n = \{8, 10, 12\}$.

In view of the staggering of the results our extrapolated $\text{SUB}\infty$ - ∞ results for M , which are shown in Fig. 5 are based on the $\text{SUB}n$ - n data set $n = \{2, 6, 10\}$ as input to the scheme of Eq. (35), which is the appropriate scheme when κ is appreciable, and especially near any QCPs at which M vanishes. The corresponding values where $M \rightarrow 0$ for the extrapolated curves are thus also those shown in Fig. 4 on the extrapolated GS energy per spin curves by the plus (+) symbols. They hence provide us with our best estimates so far for the two QCPs, viz., κ_{c_1} above which Néel order melts, and κ_{c_2} below which Néel-II order similarly melts. Using the extrapolation scheme of Eq. (35) and the input $\text{SUB}n$ - n data sets $n = \{2, 6, 10\}$ for the two model states provides the values $\kappa_{c_1} \approx 0.248$ and $\kappa_{c_2} \approx 0.343$, with clear evidence for an intermediate state in the range $\kappa_{c_1} < \kappa < \kappa_{c_2}$.

Before we proceed to investigate the intermediate regime further it is worth pausing for a moment to consider the accuracy of our results using the necessarily restricted set of $\text{SUB}n$ - n data points with $n = \{2, 6, 10\}$ only. To do so it is perhaps sufficient to consider the case $\kappa = 0$ only, where the extrapolation scheme of Eq. (34) is the apposite one for M . Precisely in the unfrustrated limit, $\kappa = 0$, the $(4m - 2)/4m$ staggering effect, seen in the raw $\text{SUB}n$ - n results $M(n)$ for values of κ appreciably far from $\kappa = 0$, essentially disappears. Thus, precisely at $\kappa = 0$ we may also use the $\text{SUB}n$ - n data set $n = \{4, 6, 8, 10\}$, which, *a priori*, should provide a much more robust result than using the restricted set $n = \{2, 6, 10\}$. For the GS energy per spin we obtain values $E(\kappa = 0)/N \approx -1.83063$ using the restricted set $n = \{2, 6, 10\}$, which may be compared with the corresponding value $E(\kappa = 0)/N \approx -1.83061$ using the set $n = \{4, 6, 8, 10\}$ (which is also the value quoted in Ref. [80]). Similarly, for the magnetic order parameter we find, using Eq. (34), $M(\kappa = 0) \approx 0.7441$ using the restricted set $n = \{2, 6, 10\}$, and $M(\kappa = 0) \approx 0.7412$ [80] using the set $n = \{4, 6, 8, 10\}$. Clearly, the very close agreement between the respective pairs of values lends considerable credence to our results for M at arbitrary

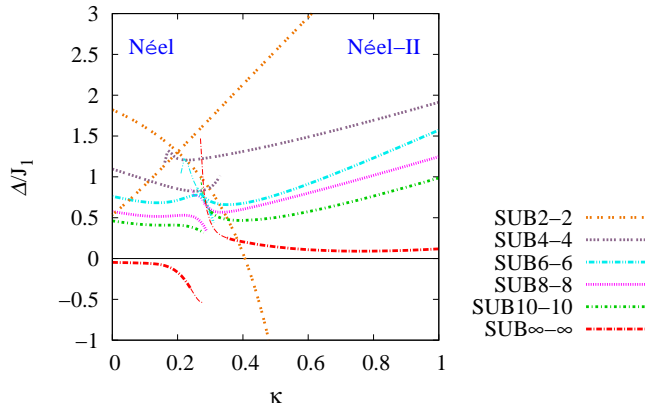


FIG. 6. (Color online) CCM results for spin gap Δ (in units of J_1) versus the frustration parameter $\kappa \equiv J_2/J_1$, for the spin-1 J_1 - J_2 model on the honeycomb lattice (with $J_1 > 0$). Results based on both the Néel and Néel-II states as the CCM model states are shown in $\text{SUB}n$ - n approximations with $n = \{2, 4, 6, 8, 10\}$, together with the corresponding $\text{SUB}\infty$ - ∞ extrapolation using Eq. (36), with the data sets $n = \{2, 6, 10\}$. Those portions of the curves with thinner lines indicate the respective unphysical regions where $M < 0$.

values of κ , and also to the values for the QCPs, κ_{c_1} and κ_{c_2} , so obtained.

We turn our attention next to the triplet spin gap Δ . In Fig. 6 we show our $\text{SUB}n$ - n approximants with $n = \{2, 4, 6, 8, 10\}$, again based on both the Néel and Néel-II quasiclassical AFM states as CCM model states. A similar $(4m - 2)/4m$ staggering of the curves to that seen in Fig. 5 for the magnetic order parameter M is also clearly visible in Fig. 6 for the corresponding curves for the spin gap Δ . We thus again show the corresponding $\text{SUB}\infty$ - ∞ extrapolations, based now on Eq. (36) to obtain the value d_0 , using the two restricted sets of $\text{SUB}n$ - n approximants with $n = \{2, 6, 10\}$ as input data. As is completely to be expected from states with magnetic LRO, and hence with gapless Goldstone magnon modes, our results are compatible, within very small numerical errors, with $\Delta = 0$ in the two regions $\kappa < \kappa_{c_1}$ and $\kappa > \kappa_{c_2}$ with the values κ_{c_1} and κ_{c_2} as determined above from the points at which $M \rightarrow 0$.

However, the most striking feature of Fig. 6 is the quite different behavior of the respective curves for Δ at the two critical points κ_{c_1} and κ_{c_2} . Thus, for example, near the lower termination point κ_{c_2} of the Néel-II phase all of the $\text{SUB}n$ - n curves (with $n > 2$), as well as the $\text{SUB}\infty$ - ∞ extrapolant shown, exhibit a clear tendency for a gapped state to open up below the QCP at κ_{c_2} . By contrast, near the upper termination point κ_{c_1} of the Néel phase there is no such obvious tendency for a gapped state to appear immediately beyond the QCP at κ_{c_1} . The preliminary evidence from our spin gap results is thus that in the intermediate region $\kappa_{c_1} < \kappa < \kappa_{c_2}$ there are (at least) two different GS phases. The tran-

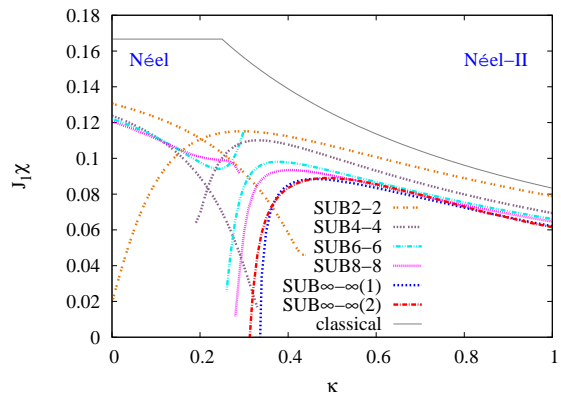


FIG. 7. (Color online) CCM results for the zero-field magnetic susceptibility χ (in units of J_1^{-1} , and where the gyromagnetic ratio $g\mu_B/\hbar = 1$) versus the frustration parameter $\kappa \equiv J_2/J_1$, for the spin-1 J_1 - J_2 model on the honeycomb lattice (with $J_1 > 0$). Results based on both the canted Néel and canted Néel-II states as CCM model states are shown in $\text{SUB}n$ - n approximations with $n = \{2, 4, 6, 8\}$, together with the corresponding $\text{SUB}\infty$ - $\infty(1)$ and $\text{SUB}\infty$ - $\infty(2)$ Néel-II extrapolations using Eqs. (39) and (38), respectively, with the data set $n = \{4, 6, 8\}$. The classical results from Eqs. (28) and (29) are also shown for comparison.

sition at κ_{c_1} appears to be from a Néel-ordered state to a gapless state, while that at κ_{c_2} appears to be between a gapped state and a state with Néel-II magnetic LRO. The precise numerical values for κ_{c_1} and κ_{c_2} are difficult to determine from the results for Δ but, from Fig. 6, they are clearly compatible with those found earlier from the results for the order parameter M .

In order to try to corroborate the above findings from the spin gap Δ , we now turn our attention to the zero-field magnetic susceptibility χ . To calculate χ within the CCM we now use the canted Néel and Néel-II states shown in Figs. 3(a) and 3(b), respectively, as model states. In view of the lower symmetries of these states in comparison with their zero-field counterparts in Figs. 1(a) and 1(b), respectively, the numbers $N_f(n)$ of fundamental CCM configurations at a given $\text{SUB}n$ - n level of approximation are considerably greater for χ than those for the GS parameters E/N and M . For example, for the canted Néel (canted Néel-II) model state for the present spin-1 model, we have $N_f(8) = 59517$ (177358) at the respective $\text{SUB}8$ -8 levels. Thus, whereas for the zero-field Néel and Néel-II model states we are able to perform $\text{SUB}n$ - n calculations for the parameters E/N and M with $n \leq 10$, for the corresponding canted states we are only able to perform $\text{SUB}n$ - n calculations for χ with $n \leq 8$. Figure 7 displays the corresponding results obtained.

Once again we see that there is a marked difference in the behavior of the curves near the two QCPs at κ_{c_1} and κ_{c_2} . Firstly, on the Néel-II side, each of the $\text{SUB}n$ - n curves exhibits a sharp downturn near its respective termination point. Although there appears to be some

possible $(4m - 2)/4m$ staggering of the results around the region close to κ_{c_2} , it is both much less marked for higher values of κ and much less evident than for the corresponding results for either M or Δ . Thus, in Fig. 7, we also show for the Néel-II results extrapolations using the data set $n = \{4, 6, 8\}$. For comparison purposes we show separate extrapolations based on each of Eqs. (38) and (39). The two extrapolations are clearly in very close agreement with one another except in a very small region near the QCP at κ_{c_2} , which is where the exponent ν in the fit of the form of Eq. (38) also differs appreciably from the value 1, which is appropriate for Eq. (39). Thus, in the critical region where χ becomes small the SUB ∞ - ∞ (1) fit based on Eq. (39) must clearly be preferred, and the value of κ at which $\chi \rightarrow 0$ for this fit is $\kappa \approx 0.337$. This value is in excellent agreement with the corresponding value $\kappa_{c_2} \approx 0.343$ at which $M^{\text{Néel-II}} \rightarrow 0$ from Fig. 5 (Note that even the corresponding value of $\kappa \approx 0.313$ obtained from the less justified SUB ∞ - ∞ (2) fit in Fig. 7 is remarkably close to the value of κ_{c_2} obtained from the vanishing of the Néel-II LRO.) As we have noted before, the vanishing of χ in a quantum spin model is a very clear signal of a transition at that point to a gapped state [60, 61]. Hence, the results for χ lend weight to our corresponding results for Δ that the transition at $\kappa_{c_2} \approx 0.34$ is between a state with Néel-II magnetic LRO and a gapped state.

Secondly, by contrast with the Néel-II results for χ , the Néel results behave markedly differently near their respective termination points in Fig. 7. Thus, on the Néel side, whereas the lower-order SUB n - n curves with $n = \{2, 4\}$ exhibit a downturn near their termination points, this feature disappears for the higher-order counterparts, $n = \{6, 8\}$. Hence, the results shown in Fig. 7 for the Néel side cannot readily be extrapolated. What is indubitably clear, however, from the most accurate results with the higher values of the SUB n - n truncation index n , is that there is no tendency at all for χ to vanish as the Néel order melts, thereby providing further evidence for the QPT at κ_{c_1} being to a gapless state. Furthermore, the SUB n - n results with $n = \{6, 8\}$, based on the Néel state as CCM model state, are completely compatible with the same value $\kappa_{c_1} \approx 0.25$ as found from the vanishing of the Néel magnetic LRO parameter M .

For further evidence of the QPT at κ_{c_1} we also show in Fig. 8 our CCM results for the spin stiffness coefficient ρ_s based on the twisted Néel state of Fig. 2 as our choice of model state $|\Phi\rangle$. Once again, just as for the magnetic susceptibility, χ , the reduced symmetry of the twisted model state increases the number $N_f(n)$ of fundamental CCM configurations at a given SUB n - n level from that using its untwisted GS counterpart. For example, for the twisted Néel model state for the present spin-1 honeycomb-lattice model, we have $N_f(8) = 352515$ at the SUB8-8 level. Just as for χ , we are thus only able to perform SUB n - n calculations for ρ_s with $n \leq 8$. The results are displayed in Fig. 8.

While the SUB n - n data points fit well to the extrap-

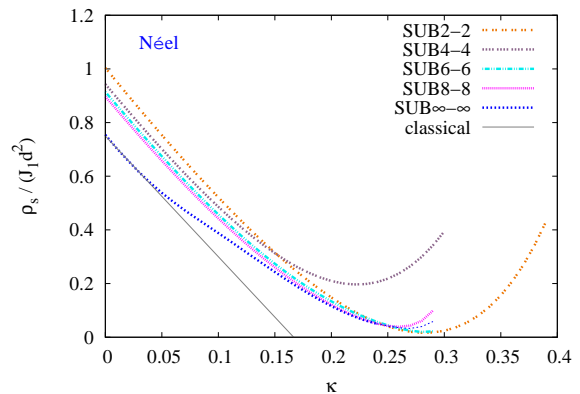


FIG. 8. (Color online) CCM results for the spin stiffness coefficient ρ_s (in units of $J_1 d^2$) versus the frustration parameter $\kappa \equiv J_2/J_1$, for the spin-1 J_1 - J_2 model on the honeycomb lattice (with $J_1 > 0$). Results based on the Néel state as CCM model state are shown in SUB n - n approximations with $n = \{2, 4, 6, 8\}$, together with the corresponding SUB ∞ - ∞ extrapolation using Eq. (39), with the data set $n = \{4, 6, 8\}$. That portion of the curve with a thinner line indicates the respective unphysical region where $M < 0$. The classical result from Eq. (24), $s = 1$, is also shown for comparison.

olation scheme of Eq. (37) at or very near to the unfrustrated limit $\kappa = 0$, the curves again exhibit crossings associated with the aforementioned $(4m - 2)/4m$ staggering. This makes extrapolation somewhat problematic. However, in Fig. 8 we again use the unbiased scheme of Eq. (39) with the data set $n = \{4, 6, 8\}$. The corresponding SUB ∞ - ∞ curve is deemed to be reliable except in a small region around $\kappa \approx 0.25$ where the SUB6-6 and SUB8-8 curves cross, which is also where the order parameter M vanishes. Nevertheless, it is apparent from both the SUB ∞ - ∞ curve and the higher-order raw SUB n - n curves with $n = \{6, 8\}$ that the exact $\rho_s^{\text{Néel}}(\kappa)$ curve is likely to approach zero, with a zero slope, at a critical point very close to $\kappa = 0.25$. Again, this value is in keeping with the QCP κ_{c_1} obtained from the vanishing of the Néel magnetic order parameter $M^{\text{Néel}}$.

All of our results so far thus point towards the existence of both a gapless and a gapped state in the intermediate regime, $\kappa_{c_1} < \kappa < \kappa_{c_2}$, with the transition at κ_{c_1} being from a state with Néel magnetic LRO to a gapless paramagnetic state, and that at κ_{c_2} being from a gapped paramagnetic state to one with Néel-II magnetic LRO. The most important open questions are (i) what is the nature of each of these paramagnetic states, and (ii) what is the critical value κ_c^i of the intermediate QCP between the gapless and gapped paramagnetic states?

Clear candidates for the gapped state in the intermediate regime are magnetically disordered VBC states, evidence for which we may now also investigate within the CCM formalism. To that end we introduce a generalized susceptibility χ_F , which is designed to measure the (linear) response of our system to an imposed (infinitesimal) external field, described by the operator F . In order to do

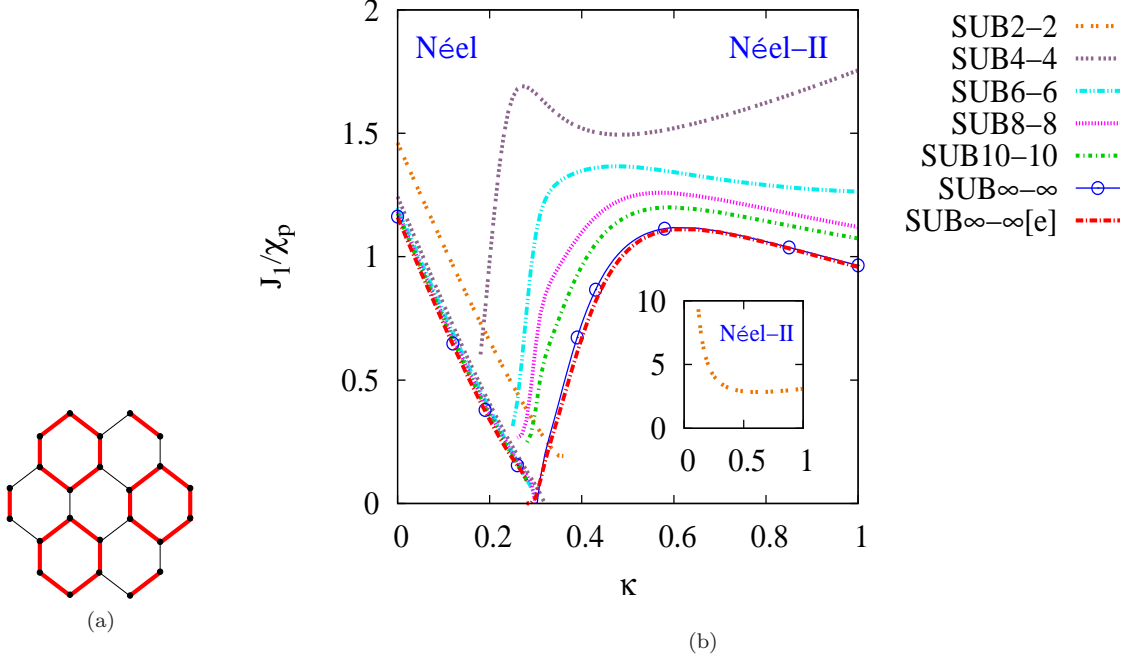


FIG. 9. (Color online) (a) The field $F = \delta\hat{O}_p$ for the plaquette susceptibility χ_p . Thick (red) and thin (black) lines correspond respectively to strengthened and weakened NN exchange couplings, where $\hat{O}_p = \sum_{\langle i,j \rangle} a_{ij} \mathbf{s}_i \cdot \mathbf{s}_j$, and the sum runs over all NN bonds, with $a_{ij} = +1$ and -1 for thick (red) and thin (black) lines respectively. (b) CCM results for the inverse plaquette susceptibility, $1/\chi_p$, (in units of J_1^{-1}) versus the frustration parameter $\kappa \equiv J_2/J_1$, for the spin-1 J_1 - J_2 model on the honeycomb lattice (with $J_1 > 0$). Results based on both the Néel and Néel-II states as CCM model states are shown in SUB n - n approximations with $n = \{2, 4, 6, 8, 10\}$, together with the corresponding SUB ∞ - ∞ [e] and SUB ∞ - ∞ extrapolations using Eqs. (42) and (43), respectively, with the data sets $n = \{2, 6, 10\}$.

so we thus add to our Hamiltonian H of Eq. (1) an extra field term $F = \delta\hat{O}_F$, where \hat{O}_F is an operator that breaks some symmetry of H , and δ is simply the (infinitesimal) strength parameter. We will choose F here to represent various forms of VBC order, as we describe more fully below. The energy per spin, $E(\delta)/N \equiv e(\delta)$ is then calculated, using the same CCM technology as before and based on either the previous Néel or Néel-II model states, for the (infinitesimally) perturbed Hamiltonian $H + F$. The generalized susceptibility is then defined as

$$\chi_F \equiv - \left. \frac{\partial^2 e(\delta)}{\partial \delta^2} \right|_{\delta=0}, \quad (40)$$

and the energy per spin,

$$e(\delta) = e_0 - \frac{1}{2}\chi_F\delta^2 + O(\delta^4), \quad (41)$$

is a maximum at $\delta = 0$ for $\chi_F > 0$. A clear signal of the system becoming unstable against the perturbing field F is then the divergence of χ_F or, equivalently, the finding that χ_F^{-1} become zero (and then possibly changes sign) at some critical value of the frustration parameter κ .

Clearly our computed CCM SUB n - n estimates for any such susceptibility χ_F need, as usual, to be extrapolated

to be SUB ∞ - ∞ limit. There are various ways in practice to do so. The most direct way is obviously to extrapolated first our SUB n - n results for the perturbed energy per spin, $e^{(n)}(\delta)$, before using them to calculate χ_F via Eq. (40) or, in practice, Eq. (41). A similar scheme to Eq. (32) for the GS energy, viz., one with a leading power $1/n^2$, typically works well except in regions near to a QCP. Since we are especially interested in using χ_F precisely in such regions, we prefer [83, 84] to use an unbiased scheme of the form of Eq. (39), namely,

$$e^{(n)}(\delta) = e_0(\delta) + e_1(\delta)n^{-\nu}, \quad (42)$$

in which the leading exponent ν is a fitting parameter along with the linear parameters $e_0(\delta)$ and $e_1(\delta)$. In this way the extrapolated, so-called SUB ∞ - ∞ [e], value $e_0(\delta)$ is then used to calculate χ_F via Eq. (41). As an alternative method, a corresponding direct extrapolation scheme for the SUB n - n estimates, $\chi_F^{-1}(n)$, of the inverse susceptibility, of the form

$$\chi_F^{-1}(n) = x_0 + x_1n^{-2} + x_2n^{-4}, \quad (43)$$

has also been found previously (and see, e.g., Refs. [19, 83] to give consistently reliable results, again with the

possible exception of critical regions where χ_F^{-1} becomes small or zero. In the results presented below we will use both the schemes of Eqs. (42) and (43) in our plots of χ_F^{-1} as a function of κ , in order to test the reliability of the extrapolation procedures.

Since strong evidence for a state with PVBC order has been found within the corresponding region $\kappa_{c_1} < \kappa < \kappa_{c_2}$ of the spin- $\frac{1}{2}$ version of the present J_1 - J_2 model on the honeycomb lattice, as reviewed in Sec. II, it is perhaps natural to choose first the perturbing operator F to promote PVBC order, as illustrated in Fig. 9(a). It clearly breaks the translational symmetry of the system. Despite the reduced symmetry of the perturbed Hamiltonian, $H + F$, we are still able to perform SUB n - n calculations for the corresponding plaquette susceptibility χ_p for values of the truncation parameter $n \leq 10$, using both the Néel and Néel-II quasiclassical AFM states as our CCM model states. The corresponding SUB n - n results for χ_p^{-1} as a function of κ are shown in Fig. 9(b). They clearly also demonstrate a $(4m - 2)/4m$ staggering of the sort seen previously for other GS parameters. Hence, in Fig. 9(b) we also show extrapolated results using our SUB n - n data with $n = \{2, 6, 10\}$ and both schemes of Eqs. (42) and (43).

It is evident that both schemes give results that are in excellent agreement with one another. Furthermore, the strong collective evidence is that χ_p^{-1} goes to zero only at a single point, $\kappa \approx 0.30$, on *both* the Néel and Néel-II sides. On the Néel side the SUB10-10 data actually terminates slightly below this value, but the two SUB ∞ - ∞ curves shown both clearly would reach $\chi_p^{-1} = 0$ at the value of $\kappa \approx 0.30$ when extrapolated the small extra necessary distance. Clearly, on the Néel side χ_p^{-1} does not vanish at the point $\kappa_{c_1} \approx 0.25$ at which Néel LRO actually vanishes, as measured by $M^{\text{Néel}} \rightarrow 0$. Similarly, on the Néel-II side the SUB ∞ - ∞ curve based on Eq. (43) reaches the value zero at the value $\kappa \approx 0.303$. While the Néel-II SUB ∞ - ∞ [e] curve based on Eq. (42) shows a very slight tendency to flatten near the point where χ_p^{-1} goes to zero, it too reaches zero at $\kappa \approx 0.29$.

All of these results are in accord with our previous findings that (a) the Néel order vanishes at a QCP κ_{c_1} at which a magnetically disordered gapless state appears; (b) this gapless state itself disappears at a QCP κ_c^i at which a magnetically disordered gapped state appears; and (c) this gapped state disappears at a QCP κ_{c_2} , above which a magnetically ordered state with Néel-II LRO appears. The additional evidence from all of the PVBC results shown is that χ_p^{-1} vanishes only at a single point, $\kappa_c^i \approx 0.30$ at which a gapped state appears, but that this gapped state, which is expected to be stable over the region $\kappa_c^i < \kappa < \kappa_{c_2}$, is not one with PVBC order, since $1/\chi_p^{\text{Néel-II}}$ shows essentially no tendency to vanish in this interval.

Another state with VBC order that has been associated with the spin- $\frac{1}{2}$ version of the present model is the SDVBC (or lattice nematic) state illustrated in Fig. 10(a). It is formed from the Néel-II state by replacing all

of the parallel NN spin pairs by spin-singlet dimers. Just like the Néel-II state, so does the SDVBC state break the lattice rotational symmetry. Once again, we may test for the susceptibility of our system to form a state with SDVBC order by now choosing the perturbing operator to promote SDVBC order, $F \rightarrow \delta O_d$, as illustrated in Fig. 10(a). Again, we are able to perform SUB n - n calculations for the corresponding staggered dimer susceptibility χ_d , for values of the truncation parameter $n \leq 10$, and with the CCM model state chosen as either the Néel or the Néel-II state, despite the reduced symmetry of the perturbed Hamiltonian, $H + F$. The corresponding SUB n - n results for χ_d^{-1} as a function of κ are shown in Fig. 10(b). Unsurprisingly by now, they also illustrate a $(4m - 2)/4m$ staggering effect, and hence in Fig. 10(b) the two sets of extrapolations, based on Eqs. (42) and (43), are shown based on the SUB n - n data sets with $n = \{2, 6, 10\}$.

Just as for the corresponding extrapolated PVBC results in Fig. 9(b), so now do both extrapolation schemes for the SDVBC results, agree very well with one another. The SDVBC for χ_d^{-1} results based on the Néel model state are completely consistent and analogous with the corresponding PVBC results for χ_p^{-1} . Again, both the SUB ∞ - ∞ and SUB ∞ - ∞ [e] curves shown would reach $\chi_d^{-1} = 0$ at the value $\kappa \approx 0.30$ when extrapolated the small extra needed amount. However, by contrast, the SDVBC results based on the Néel-II state for χ_d^{-1} are now qualitatively different from the corresponding PVBC results for χ_p^{-1} on the Néel-II side. Thus, all of the SDVBC results for χ_d^{-1} based on the Néel-II model state, both the “raw” SUB n - n curves and the two extrapolations shown, exhibit a clear tendency to flatten near the critical point where they become zero, and then remain zero over a finite range of values of κ below the corresponding critical value. Thus, for example, the SUB ∞ - ∞ curve for $1/\chi_d^{\text{Néel-II}}$, based on Eq. (43), touches zero at a value $\kappa \approx 0.32$ with a slope very close to zero, while the corresponding SUB ∞ - ∞ [e] curve, based on Eq. (42), is clearly zero within small numerical uncertainties over a range of values $0.29 \lesssim \kappa \lesssim 0.33$. Thus we may now identify the gapped state as likely having SDVBC order, and the range of values of κ for which $\chi_d^{-1} = 0$ as being the range $\kappa_c^i < \kappa < \kappa_{c_2}$. From both the PVBC and SDVBC results, we estimate $\kappa_c^i \approx 0.30$, while the SDVBC results for $1/\chi_d^{\text{Néel-II}}$ yield the estimate $\kappa_{c_2} \approx 0.33$. This latter value is in complete agreement with the corresponding estimate, $\kappa_{c_2} \approx 0.34$, at which Néel-II LRO vanishes, as measured by the point where $M^{\text{Néel-II}} \rightarrow 0$. Clearly, the latter value is intrinsically more accurate, however, than that obtained from the point where $1/\chi^{\text{Néel-II}} \rightarrow 0$, due to the totally different slopes of the curves at their respective (vanishing) critical points.

In the concluding section we now summarize and discuss our results.

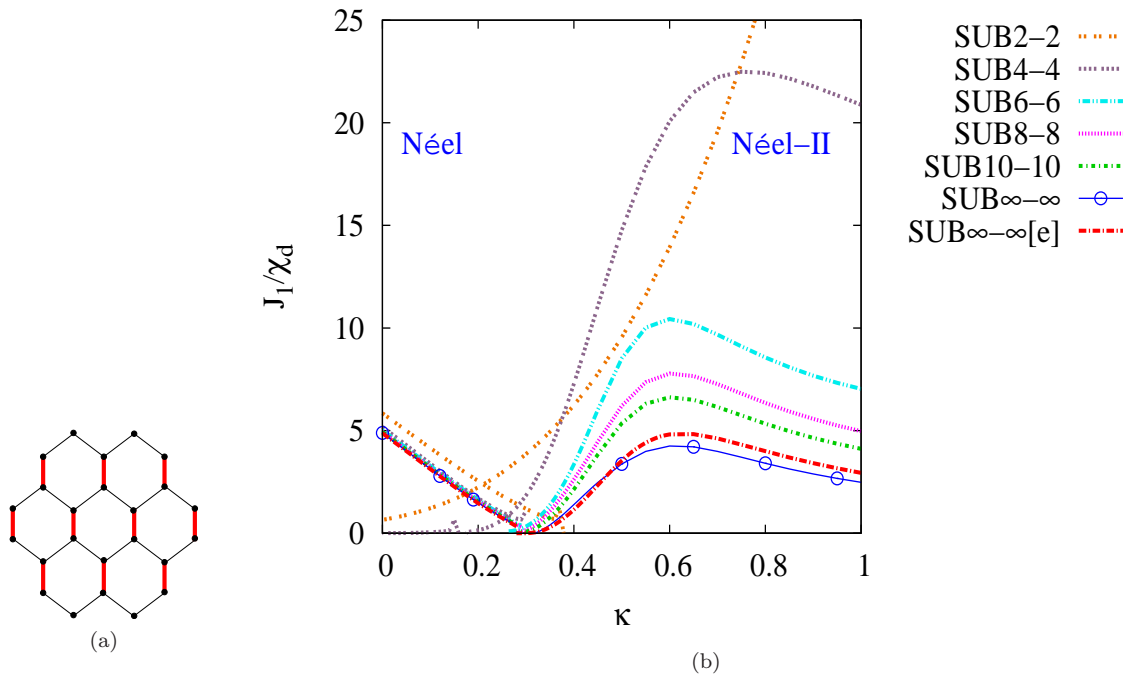


FIG. 10. (Colour online) (a) The field $F = \delta \hat{O}_d$ for the staggered dimer susceptibility, χ_d . Thick (red) and thin (black) lines correspond respectively to strengthened and unaltered NN exchange couplings, where $\hat{O}_d = \sum_{\langle i,j \rangle} a_{ij} \mathbf{s}_i \cdot \mathbf{s}_j$, and the sum runs over all NN bonds, with $a_{ij} = +1$ and 0 for thick (red) lines and thin (black) lines respectively. (b) CCM results for the inverse staggered dimer susceptibility, $1/\chi_d$, (in units of J_1^{-1}) versus the frustration parameter, $\kappa \equiv J_2/J_1$, for the spin-1 J_1 - J_2 model on the honeycomb lattice (with $J_1 > 0$). Results based on both the Néel and Néel-II states as CCM model states are shown in SUB n - n approximations with $n = \{2, 4, 6, 8, 10\}$, together with the corresponding SUB ∞ - ∞ [e] and SUB ∞ - ∞ extrapolations using Eqs. (42) and (43), respectively, with the data sets $n = \{2, 6, 10\}$.

V. DISCUSSION AND CONCLUSIONS

To summarize, we have applied the CCM in this paper, at high orders of approximation, to the spin-1 J_1 - J_2 Heisenberg antiferromagnet on the honeycomb lattice, in the case of AFM NN bonds ($J_1 > 0$) and AFM NNN bonds ($J_2 \equiv \kappa J_1 > 0$), in the range $0 \leq \kappa \leq 1$ of the frustration parameter. In particular, our aim has been to present a comprehensive analysis of the GS ($T = 0$) quantum phase diagram of the model. To that end we have calculated the GS energy, the magnetic order parameter, the zero-field transverse magnetic susceptibility, and the spin stiffness coefficient for two quasiclassical AFM states with Néel and Néel-II forms of LRO. We have also calculated their generalized susceptibilities against the formation of two forms of VBC order. A distinct advantage of the CCM, in which all of these quantities are calculated within a unified framework, is that all of the calculations are anchored from the outset in the thermodynamic limit of an infinite lattice ($N \rightarrow \infty$). Unlike many alternate accurate techniques (e.g., the DMRG method), the CCM thereby obviates the need for any finite-size scaling or extrapolation to the bulk limit, which is often the step that is most uncontrolled in practice.

Nevertheless, it is perhaps worthwhile at this point to reflect again on two key aspects of the CCM that are inherent to it, namely (a) the precise role of the (reference or) model state, and (b) the fact that while the method is certainly (bi-)variational, the lack of manifest Hermiticity between the parametrized corresponding bra and ket states implies that the method does not provide strict upper bounds to the GS energy. Thus, firstly, while the formal role of $|\Phi\rangle$ as a cyclic vector with respect to an appropriate set of mutually commuting, multiconfigurational creation operators $\{C_I^+\}$ has been fully expounded in Sec. III, one may legitimately enquire as to whether the results obtained in practice are truly independent of the choice of model state, or whether some inherent bias remains. In other words, are the physical scenarios implied by the zero-temperature, quantum phase diagram that we have obtained by the CCM, independent of the choices of model state?

While it is perhaps difficult to be absolutely, categorically affirmative on this point, in practice the answer has always been found to be yes. Thus, for example, if one considers the Néel state as a reference state for a point in the phase diagram actually characterized by Néel-II order (say, for $\kappa = 0.4$), one will find, at a given SUB n - n

level of approximation, either that no solution exists or that, if one does, the corresponding Néel order vanishes (i.e., $M \leq 0$) at either the given SUB n - n level or the suitably extrapolated SUB ∞ - ∞ limit, as Fig. 4 clearly shows for the present model. Results from *many* other models confirm these findings, often quite dramatically. For example, CCM treatments of spin- $\frac{1}{2}$ J_1 - J_2 models on both the chevron-square lattice [83] and the checkerboard lattice [85] demonstrate instances where one may find SUB n - n solutions (for all values of n) using a “wrong” model state over extended ranges of values of $\kappa \equiv J_2/J_1$, but for all of which the extrapolated order parameter vanishes ($M = 0$). In both cases VBC states have been shown to be the actual, stable GS phases.

Secondly, we reiterate that for the reasons already described, neither our SUB n - n estimates for the GS energy nor the SUB ∞ - ∞ extrapolation from Eq. (32) are guaranteed to be strict upper bounds. While our final SUB ∞ - ∞ result certainly does depend on the functional form of the extrapolation, we have tested that the form of Eq. (32) is the appropriate one both in the present case and for *many* other models, by first performing an unbiased fit of the form of Eq. (39) to show that the leading exponent is accurately given by $\nu = 2$. It is worth noting too that even for alternative variational calculations, where strict upper bounds to the GS energy *are* obtained on finite-size lattice clusters, this bound may be lost when extrapolating to the thermodynamic ($N \rightarrow \infty$) limit.

For the usual variational approaches (i.e., in explicitly Hermitian schemes) the GS energy values constitute a rather well-defined figure of merit to establish which approach is more accurate. Thus, in order to avoid the finite-size extrapolation problem, comparison is usually made for a given finite-sized lattice. In this context we note that while in principle the CCM *can* be implemented for finite-size clusters, in practice it is seldom done, both since the method does not provide energy upper bounds and since it *can* be applied directly in the thermodynamic limit, which is usually of primary interest. Furthermore, as we point out below, results obtained only on finite lattices (e.g., on finite cylinders for DMRG calculations) can, and often do, as for the present model, show strong finite-size effects that may be wholly absent in the thermodynamic limit. For that reason, CCM practitioners generally regard it as a strength of the method that results are presented directly in the $N \rightarrow \infty$ limit, with no finite-size scaling, and with the extrapolation in the level of implementation the sole approximation made.

Returning to our results, the wide range of low-energy parameters examined provides us with a consistent picture of a quantum phase diagram for the model that comprises four different stable GS phases. For $\kappa < \kappa_{c_1}$ we find a quasiclassical AFM phase with Néel magnetic LRO, while for $\kappa > \kappa_{c_2}$ we find another quasiclassical AFM phase with magnetic LRO of the Néel-II type illustrated in Fig. 1(b). For intermediate values of the frustration parameter, $\kappa_{c_1} < \kappa < \kappa_{c_2}$, the ground state is one of two distinct quantum paramagnetic states, nei-

ther of which has any discernible magnetic LRO. We find that at the QCP κ_{c_1} the phase transition is from the gapless Néel state to another gapless state, while at the QCP κ_{c_2} the transition is from the gapless Néel-II state to a gapped state. The latter gapped state appears not to have PVBC order, as in the corresponding intermediate regime for the spin- $\frac{1}{2}$ version of the model. Strong evidence is presented that a more likely candidate gapped state is one with SDVBC order, which breaks the same symmetries as the state with Néel-II order. The two paramagnetic states meet at a third QCP κ_c^i , with $\kappa_{c_1} < \kappa_c^i < \kappa_{c_2}$. A careful analysis of all of the CCM results yields our best estimates for the three QCPs as $\kappa_{c_1} = 0.250(5)$, $\kappa_{c_2} = 0.340(5)$, and $\kappa_c^i = 0.305(5)$. The seemingly featureless nature of the gapless GS phase in the region $\kappa_{c_1} < \kappa < \kappa_c^i$, where both magnetic and VBC orderings vanish, clearly makes it a strong candidate to be a QSL state.

Our results may be compared to those from a recent DMRG study of the same system [35], which found a three-phase structure for the GS ($T = 0$) phase diagram. This study also found a Néel AFM phase for $\kappa < \kappa_{c_1}$, and also suggested a Néel-II AFM phase for $\kappa > \kappa_{c_2}$ (which was termed a stripe phase in Ref. [35]). The numerical values obtained for these two QCPs, $\kappa_{c_1} \approx 0.27(1)$ and $\kappa_{c_2} \approx 0.32$, are in reasonable agreement with our own findings. The DMRG study also identified an intermediate nonmagnetic phase region, in which the spin gap was found to enlarge considerably on the finite-size cylinders investigated. However, the DMRG results differ from ours in suggesting that in the entire intermediate region the GS phase has PVBC order, whereas our own results give little evidence for this form of VBC order. It is interesting to speculate about possible causes for this disagreement.

In the first place it is clear that the DMRG results for this system display rather strong finite-size effects for the cylinders that are feasible to study computationally. Two sorts of cylinder geometries are studied, viz., so-called AC m and ZC m types, with armchair and zigzag open edges respectively, and where m is the number of unit cells (i.e., the number of sites on either sublattice \mathcal{A} or sublattice \mathcal{B}) in the width direction. Both types of cylinders are considered with lengths up to 24 unit cells. For the magnetically ordered phases the DMRG calculations are performed with widths $m \leq 8$. However, in the intermediate phase it is found that convergence is sufficiently challenging that the calculations are constrained to relative narrow cylinders, $m \leq 6$.

Even in the Néel-II phase region the GS energy, extracted from the bulk bond energy on long cylinders, is different on the two types of cylinders, with the ZC cylinders giving lower energies than the AC cylinders. Thus, the spin configurations on the ZC cylinders are ordered as in the 4-sublattice Néel-II AFM phase, whereas those on the AC cylinders order on an 8-sublattice double-Néel AFM pattern (i.e., with an 8-site unit cell). The double-Néel phase comprises parallel zigzag chains of alternating

pairs of parallel spins, ordered as $\cdots \uparrow\downarrow\downarrow\uparrow\uparrow\downarrow\downarrow \cdots$, and with NN spins on neighboring chains antiparallel to one another, in such a way that each hexagonal plaquette has 3 spins pointing in each direction. It is degenerate in energy with the Néel-II phase at the classical level. When the DMRG results on long cylinders are extrapolated to the thermodynamic limit ($m \rightarrow \infty$) using results with $m = \{4, 6, 8\}$, at a value $\kappa = 0.4$, for example, the AC cylinders give a bulk value $E/(NJ_1) \approx -1.267$, while the ZC cylinders give the lower value $E/(NJ_1) \approx -1.274$. Since the two geometries should presumably give the same energy in the thermodynamic limit, these different values indicate the strong finite-size effects on the (relatively small) systems that can be studied with available computational resources. By comparison, our own extrapolated energy at $\kappa = 0.4$ is $E/(NJ_1) \approx -1.2748$ based on an extrapolation using Eq. (32) from SUB n - n calculations based on the Néel-II model state with $n = \{2, 6, 10\}$. It is in excellent agreement with the DMRG results on ZC cylinders, which also exhibit Néel-II ordering at $\kappa = 0.4$.

Turning to the intermediate region, the DMRG calculations are even more constrained. On the AC4 and ZC4 cylinders the bond energies are found to be quite uniform in the bulk of the cylinder, and in order to detect any lattice symmetry breaking it is necessary to go to wider systems, for which convergence can be achieved only for the AC6 and ZC6 cylinders. It is based only on these cylinders that PVBC ordering is suggested, even though the truncation errors are considerably larger than for the corresponding results in the Néel and Néel-II regions.

From our own results shown in Figs. 9 and 10, it is also

interesting to note that for most values of κ , except in a small region around $\kappa = 0.3$ (near the QCP κ_{c2}), the system is actually *more* susceptible to PVBC ordering than to SDVBC ordering, i.e., $\chi_p^{-1} < \chi_d^{-1}$. It is only in the very narrow region $\kappa_c^i < \kappa < \kappa_{c2}$ that SDVBC ordering clearly dominates over PVBC ordering. Given these results, and the strong finite-size effects observed in the DMRG results as discussed above, it is entirely possible that the PVBC ordering observed on the relatively narrow cylinders for which calculations are feasible in the intermediate region $\kappa_{c1} < \kappa < \kappa_{c2}$ would itself give way to other forms of order on wider cylinders.

To conclude, it is clear that the competition between different phases in the intermediate region $\kappa_{c1} < \kappa < \kappa_{c2}$ for the spin-1 J_1 - J_2 model on the honeycomb lattice is delicate and subtle. While our own results show rather clear evidence of two intermediate phases, viz., a gapped phase with probable SDVBC order in the interval $\kappa_c^i < \kappa < \kappa_{c2}$, and a gapless paramagnetic phase in the interval $\kappa_{c1} < \kappa < \kappa_c^i$ (which is a possible QSL), it would be very useful for other methods to be applied to this system to confirm our results.

ACKNOWLEDGMENTS

We thank the University of Minnesota Supercomputing Institute for the grant of supercomputing facilities, on which the work reported here was performed. One of us (RFB) gratefully acknowledges the Leverhulme Trust (United Kingdom) for the award of an Emeritus Fellowship (EM-2015-007).

-
- [1] J. Villain, J. Phys. (France) **38**, 385 (1977).
 - [2] J. Villain, R. Bidaux, J.-P. Carton, and R. Conte, J. Phys. (France) **41**, 1263 (1980).
 - [3] E. F. Shender, Zh. Eksp. Teor. Fiz. **83**, 326 (1982), [Sov. Phys. JETP **56**, 178 (1982)].
 - [4] C.-M. Jian and M. Zaletel, Phys. Rev. B **93**, 035114 (2016).
 - [5] E. Lieb, T. Schultz, and D. Mattis, Ann. Phys. (N. Y.) **16**, 407 (1961).
 - [6] M. B. Hastings, Phys. Rev. B **69**, 104431 (2004).
 - [7] M. Oshikawa, Phys. Rev. Lett. **84**, 1535 (2000).
 - [8] F. D. M. Haldane, Phys. Rev. Lett. **61**, 1029 (1988).
 - [9] N. Read and S. Sachdev, Phys. Rev. B **42**, 4568 (1990).
 - [10] N. D. Mermin and H. Wagner, Phys. Rev. Lett. **17**, 1133 (1966).
 - [11] E. Rastelli, A. Tassi, and L. Reatto, Physica B & C **97**, 1 (1979).
 - [12] A. Mattsson, P. Fröjdh, and T. Einarsson, Phys. Rev. B **49**, 3997 (1994).
 - [13] J. B. Fouet, P. Sindzingre, and C. Lhuillier, Eur. Phys. J. B **20**, 241 (2001).
 - [14] A. Mulder, R. Ganesh, L. Capriotti, and A. Paramekanti, Phys. Rev. B **81**, 214419 (2010).
 - [15] F. Wang, Phys. Rev. B **82**, 024419 (2010).
 - [16] D. C. Cabra, C. A. Lamas, and H. D. Rosales, Phys. Rev. B **83**, 094506 (2011).
 - [17] R. Ganesh, D. N. Sheng, Y.-J. Kim, and A. Paramekanti, Phys. Rev. B **83**, 144414 (2011).
 - [18] B. K. Clark, D. A. Abanin, and S. L. Sondhi, Phys. Rev. Lett. **107**, 087204 (2011).
 - [19] D. J. J. Farnell, R. F. Bishop, P. H. Y. Li, J. Richter, and C. E. Campbell, Phys. Rev. B **84**, 012403 (2011).
 - [20] J. Reuther, D. A. Abanin, and R. Thomale, Phys. Rev. B **84**, 014417 (2011).
 - [21] A. F. Albuquerque, D. Schwandt, B. Hetényi, S. Capponi, M. Mambrini, and A. M. Läuchli, Phys. Rev. B **84**, 024406 (2011).
 - [22] H. Mosadeq, F. Shahbazi, and S. A. Jafari, J. Phys.: Condens. Matter **23**, 226006 (2011).
 - [23] J. Oitmaa and R. R. P. Singh, Phys. Rev. B **84**, 094424 (2011).
 - [24] F. Mezzacapo and M. Boninsegni, Phys. Rev. B **85**, 060402(R) (2012).
 - [25] P. H. Y. Li, R. F. Bishop, D. J. J. Farnell, J. Richter, and C. E. Campbell, Phys. Rev. B **85**, 085115 (2012).
 - [26] R. F. Bishop, P. H. Y. Li, D. J. J. Farnell, and C. E. Campbell, J. Phys.: Condens. Matter **24**, 236002 (2012).
 - [27] R. F. Bishop and P. H. Y. Li, Phys. Rev. B **85**, 155135 (2012).

- [28] P. H. Y. Li, R. F. Bishop, D. J. J. Farnell, and C. E. Campbell, *Phys. Rev. B* **86**, 144404 (2012).
- [29] R. F. Bishop, P. H. Y. Li, and C. E. Campbell, *J. Phys.: Condens. Matter* **25**, 306002 (2013).
- [30] R. Ganesh, J. van den Brink, and S. Nishimoto, *Phys. Rev. Lett.* **110**, 127203 (2013).
- [31] Z. Zhu, D. A. Huse, and S. R. White, *Phys. Rev. Lett.* **110**, 127205 (2013).
- [32] H. Zhang and C. A. Lamas, *Phys. Rev. B* **87**, 024415 (2013).
- [33] S.-S. Gong, D. N. Sheng, O. I. Motrunich, and M. P. A. Fisher, *Phys. Rev. B* **88**, 165138 (2013).
- [34] X.-L. Yu, D.-Y. Liu, P. Li, and L.-J. Zou, *Physica E* **59**, 41 (2014).
- [35] S.-S. Gong, W. Zhu, and D. N. Sheng, *Phys. Rev. B* **92**, 195110 (2015).
- [36] Y. Miura, R. Hirai, Y. Kobayashi, and M. Sato, *J. Phys. Soc. Jpn.* **75**, 084707 (2006).
- [37] V. Kataev, A. Möller, U. Löw, W. Jung, N. Schittner, M. Kriener, and A. Freimuth, *J. Magn. Magn. Mater.* **290–291**, 310 (2005).
- [38] A. A. Tsirlin, O. Janson, and H. Rosner, *Phys. Rev. B* **82**, 144416 (2010).
- [39] E. Climent-Pascual, P. Norby, N. Andersen, P. Stephens, H. Zandbergen, J. Larsen, and R. Cava, *Inorg. Chem.* **51**, 557 (2012).
- [40] Y. Singh and P. Gegenwart, *Phys. Rev. B* **82**, 064412 (2010).
- [41] X. Liu, T. Berlijn, W.-G. Yin, W. Ku, A. Tsvetik, Y.-J. Kim, H. Gretarsson, Y. Singh, P. Gegenwart, and J. P. Hill, *Phys. Rev. B* **83**, 220403(R) (2011).
- [42] Y. Singh, S. Manni, J. Reuther, T. Berlijn, R. Thomale, W. Ku, S. Trebst, and P. Gegenwart, *Phys. Rev. Lett.* **108**, 127203 (2012).
- [43] S. K. Choi, R. Coldea, A. N. Kolmogorov, T. Lancaster, I. I. Mazin, S. J. Blundell, P. G. Radaelli, Y. Singh, P. Gegenwart, K. R. Choi, S.-W. Cheong, P. J. Baker, C. Stock, and J. Taylor, *Phys. Rev. Lett.* **108**, 127204 (2012).
- [44] L. P. Regnault and J. Rossat-Mignod, in *Magnetic Properties of Layered Transition Metal Compounds*, edited by L. J. De Jongh (Kluwer Academic Publishers, Dordrecht, 1990) pp. 271–321.
- [45] J. H. Roudebush, N. H. Andersen, R. Ramlau, V. O. Garlea, R. Toft-Petersen, P. Norby, R. Schneider, J. N. Hay, and R. J. Cava, *Inorg. Chem.* **52**, 6083 (2013).
- [46] T. Senthil, A. Vishwanath, L. Balents, S. Sachdev, and M. P. A. Fisher, *Science* **303**, 1490 (2004).
- [47] T. Senthil, L. Balents, S. Sachdev, A. Vishwanath, and M. P. A. Fisher, *Phys. Rev. B* **70**, 144407 (2004).
- [48] H. Kümmel, K. H. Lührmann, and J. G. Zabolitzky, *Phys Rep.* **36C**, 1 (1978).
- [49] R. F. Bishop and K. H. Lührmann, *Phys. Rev. B* **17**, 3757 (1978).
- [50] R. F. Bishop and K. H. Lührmann, *Phys. Rev. B* **26**, 5523 (1982).
- [51] J. Arponen, *Ann. Phys. (N.Y.)* **151**, 311 (1983).
- [52] R. F. Bishop and H. G. Kümmel, *Phys. Today* **40(3)**, 52 (1987).
- [53] R. J. Bartlett, *J. Phys. Chem.* **93**, 1697 (1989).
- [54] J. S. Arponen and R. F. Bishop, *Ann. Phys. (N.Y.)* **207**, 171 (1991).
- [55] R. F. Bishop, *Theor. Chim. Acta* **80**, 95 (1991).
- [56] R. F. Bishop, in *Microscopic Quantum Many-Body Theories and Their Applications*, Lecture Notes in Physics Vol. 510, edited by J. Navarro and A. Polls (Springer-Verlag, Berlin, 1998) p. 1.
- [57] C. Zeng, D. J. J. Farnell, and R. F. Bishop, *J. Stat. Phys.* **90**, 327 (1998).
- [58] D. J. J. Farnell and R. F. Bishop, in *Quantum Magnetism*, Lecture Notes in Physics Vol. 645, edited by U. Schollwöck, J. Richter, D. J. J. Farnell, and R. F. Bishop (Springer-Verlag, Berlin, 2004) p. 307.
- [59] We use the program package CCCM of D. J. J. Farnell and J. Schulenburg, see <http://www-e.uni-magdeburg.de/jschulen/ccm/index.html>.
- [60] F. Mila, *Eur. J. Phys.* **21**, 499 (2000).
- [61] B. Bernu and C. Lhuillier, *Phys. Rev. Lett.* **114**, 057201 (2015).
- [62] R. F. Bishop, D. J. J. Farnell, S. E. Krüger, J. B. Parkinson, J. Richter, and C. Zeng, *J. Phys.: Condens. Matter* **12**, 6887 (2000).
- [63] S. E. Krüger, J. Richter, J. Schulenburg, D. J. J. Farnell, and R. F. Bishop, *Phys. Rev. B* **61**, 14607 (2000).
- [64] D. J. J. Farnell, K. A. Gernoth, and R. F. Bishop, *Phys. Rev. B* **64**, 172409 (2001).
- [65] R. Darradi, J. Richter, and D. J. J. Farnell, *Phys. Rev. B* **72**, 104425 (2005).
- [66] R. Darradi, O. Derzhko, R. Zinke, J. Schulenburg, S. E. Krüger, and J. Richter, *Phys. Rev. B* **78**, 214415 (2008).
- [67] R. F. Bishop, P. H. Y. Li, R. Darradi, and J. Richter, *EPL* **83**, 47004 (2008).
- [68] R. F. Bishop, P. H. Y. Li, R. Darradi, J. Richter, and C. E. Campbell, *J. Phys.: Condens. Matter* **20**, 415213 (2008).
- [69] R. F. Bishop, P. H. Y. Li, D. J. J. Farnell, and C. E. Campbell, *Phys. Rev. B* **79**, 174405 (2009).
- [70] R. F. Bishop, P. H. Y. Li, D. J. J. Farnell, and C. E. Campbell, *Phys. Rev. B* **82**, 024416 (2010).
- [71] R. F. Bishop, P. H. Y. Li, D. J. J. Farnell, and C. E. Campbell, *Phys. Rev. B* **82**, 104406 (2010).
- [72] R. F. Bishop and P. H. Y. Li, *Eur. Phys. J. B* **81**, 37 (2011).
- [73] P. H. Y. Li and R. F. Bishop, *Eur. Phys. J. B* **85**, 25 (2012).
- [74] P. H. Y. Li, R. F. Bishop, C. E. Campbell, D. J. J. Farnell, O. Götze, and J. Richter, *Phys. Rev. B* **86**, 214403 (2012).
- [75] J. Richter, R. Zinke, and D. J. J. Farnell, *Eur. Phys. J. B* **88**, 2 (2015).
- [76] R. F. Bishop, P. H. Y. Li, O. Götze, J. Richter, and C. E. Campbell, *Phys. Rev. B* **92**, 224434 (2015).
- [77] R. F. Bishop and P. H. Y. Li, *EPL* **112**, 67002 (2015).
- [78] S. E. Krüger, R. Darradi, J. Richter, and D. J. J. Farnell, *Phys. Rev. B* **73**, 094404 (2006).
- [79] O. Götze, J. Richter, R. Zinke, and D. J. J. Farnell, *J. Magn. Magn. Mater.* **397**, 333 (2016).
- [80] R. F. Bishop and P. H. Y. Li, *J. Magn. Magn. Mater.* **407**, 348 (2016).
- [81] D. J. J. Farnell, R. Zinke, J. Schulenburg, and J. Richter, *J. Phys.: Condens. Matter* **21**, 406002 (2009).
- [82] P. H. Y. Li, R. F. Bishop, and C. E. Campbell, *Phys. Rev. B* **91**, 014426 (2015).
- [83] P. H. Y. Li, R. F. Bishop, and C. E. Campbell, *Phys. Rev. B* **88**, 144423 (2013).
- [84] R. F. Bishop, P. H. Y. Li, and C. E. Campbell, *Phys. Rev. B* **88**, 214418 (2013).

- [85] R. F. Bishop, P. H. Y. Li, D. J. J. Farnell, J. Richter, and C. E. Campbell, Phys. Rev. B **85**, 205122 (2012).